Analytical Methods

ROYAL SOCIETY OF CHEMISTRY

MINIREVIEW

View Article Online
View Journal | View Issue

Published on 14 February 2022. Downloaded by Bengal Engineering and Science University on 6/8/2022 1:03:11 PM.

Check for updates

Cite this: *Anal. Methods*, 2022, **14**, 972

Triphenylamine-based small-molecule fluorescent probes

Anirban Karak,[a] Saikat Kumar Manna [b] and Ajit Kumar Mahapatra *[a]

Received 24th January 2022
Accepted 14th February 2022

DOI: 10.1039/d2ay00134a

rsc.li/methods

Ammonia with the three hydrogens substituted by phenyls is known as triphenylamine (TPA), and is one of the most useful compounds because of its vast practical applications. Chemists have produced thousands of TPA derivatives to date. Because of its biocompatibility and structural features, it has been widely used in the fields of molecular recognition, molecular imaging, materials chemistry, and also in biology and medical science. Its strong electron-donating ability encourages scientists to produce different types of probes for molecular recognition. This review is based on recent developments and advances in TPA-based small molecular fluorescent probes within the time period 2010–2021. This extensive review may expedite improvements in more advanced fluorescent probes for vast and stimulating applications in the future.

1 Introduction

Sensing is one of the most demanding fields of application in supramolecular chemistry and has attracted researchers to develop new fluorescent probes. Different sensing mechanisms have been established so far, including photoinduced electron transfer (PET),[1] intramolecular charge transfer (ICT),[2] metal–ligand charge transfer (MLCT),[3] twisted intramolecular charge transfer (TICT),[4] electronic energy transfer (EET),[5] and fluorescence resonance energy transfer (FRET).[6] However, when designing a molecular probe to detect a particular analyte, we must consider three crucial factors: (1) high sensitivity (limit of detection), (2) high selectivity (for the very specific ion that falls under investigation) and (3) high specificity (distinguishing among other ions).[7] It is regarded as most challenging to develop a fluorescent probe with both sensitivity and selectivity properties.

Triphenylamine (TPA) is a tertiary amine consisting of three aromatic phenyl groups (Fig. 1). TPA shows very low basicity compared to its aliphatic analogue and this feature can be attributed to the resonance delocalization of the lone pair of electrons to its overall molecular structure.[8] Triphenylamine molecules and their derivatives are gaining importance in many industrial applications. Various synthetic procedures for TPA-type molecules are known. They can be prepared by the traditional method of the Ullmann condensation reaction (1903), which goes through nucleophilic attack followed by substitution of an aryl-halide in the presence of a copper catalyst and a base.[9] Again, using various catalysts like 18-crown-6-ether, $Cu(PPh_3)_3Br$, *etc.*, the traditional Ullmann reaction was adapted by researchers.[10] Recently, the utilization of palladium catalysts with phosphine ligands has been regarded as a desirable approach for the synthesis of TPA derivatives. For example, mixed secondary arylamines can be obtained from the amination of aryl halides under mild reaction conditions and with easy separation and crystallization steps.[11] Other various synthetic methods for TPA derivatives include Wittig, Stille, and Sonogashira reaction syntheses. There are numerous toxic effects of arylamines, and some of them are briefly discussed here. The primary hazards associated with exposure to arylamines are carcinogenesis and methemoglobinemia. It is the carcinogenic potential of aromatic amines that is of greater concern. The effects of exposure to TPA can be divided into two categories: acute effects and chronic effects. Acute health effects include irritation of the skin and eyes, which can occur immediately or a certain time after exposure to TPA. Chronic effects from either inhalation or skin contact can cause anoxia (pathological deficiency of oxygen), especially hypoxia caused by an impairment of the oxygen transport system in the blood.

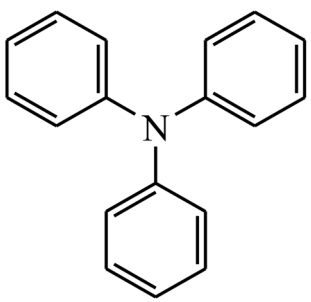

Fig. 1 Molecular structure of triphenylamine.

[a]*Department of Chemistry, Indian Institute of Engineering Science and Technology, Shibpur, Howrah-711103, West Bengal, India. E-mail: akmahapatra@chem.iiests.ac.in*

[b]*Department of Chemistry, Haldia Government College, Debhog, Purba Medinipur-721657, Haldia, West Bengal, India*

This journal is © The Royal Society of Chemistry 2022

Published on 14 February 2022. Downloaded by Bengal Engineering and Science University on 6/8/2022 1:03:11 PM.

Designing a fluorescent probe is a task in which various factors must be kept in mind. One of these factors is the ease of functionalisation of a parent molecule. Triphenylamine can be functionalised easily by various reaction techniques. TPA can be converted into the corresponding aldehyde (4-(*N*,*N*-diphenylamino)benzaldehyde) *via* the Vilsmeier–Haack reaction.[12] Again, from this aldehyde, different types of reaction can be achieved, such as Schiff-base formation by a coupling reaction between aldehyde and amine, or a Wittig reaction to form a new aldehyde. For these reactions, no extraordinary conditions are needed, so it is less expensive to functionalize TPA to form a fluorescent probe.

The molecular geometry of TPA is the result of two opposing factors. One of these two factors is the resonance stabilization of the π-electron systems and the other is the steric repulsion of protons from neighbouring phenyl groups. To enhance the delocalisation of the π-electron systems of the phenyl groups, a planar geometry (D_{3h} symmetry) is preferred, whereas steric repulsions are reduced by tilting from the molecular plane.[13,14] As a result of these two factors it possesses a propeller-like structure (C_3 symmetry).[15] TPA materials have attracted researchers' attention because of the propeller-like structural chromophore with a nitrogen atom at its centre (like a three-blade ceiling fan structure). Since the three phenyl substituents are non-coplanar, TPA derivatives can be considered as 3D systems. As a donor centre, the triphenylamine group has unique radical characteristics and large steric hindrance. The lone pair on the nitrogen of TPA plays a crucial role as a donor, so attaching very strong electron-withdrawing groups to a TPA unit results in a strong ICT. TPA can be employed in its derivative forms with different aggregation states because of C–C single bond rotation and nonplanar structure. Besides its unique structural features, its excellent quantic sensing behaviour such as limit of detection (LOD) value is also a factor for designing a TPA-based fluorescent probe over other types. Most TPA-functionalised probes have an LOD value in the ppb or ppm range. Moreover, the TPA moiety is extensively used for designing fluorescent probes because it has great chemical stability and photoluminescence property.

There are several articles on triphenylamine-based hole transport materials,[16] triphenylamine-based dyes for dye-sensitized solar cells,[17] triphenylamine-based supramolecular polymers, *etc.*[18] To the best of our knowledge, there is no systematic comprehensive review regarding triphenylamine-based fluorescent probes for sensing analytes. In this literature review we are going to focus on recent progress in triphenylamine-based fluorescent probes. We have classified these fluorescent probes into three main categories: (a) fluorescent probes for anions, (b) fluorescent probes for cations, and (c) fluorescent probes for neutral analytes. Each category is again subdivided into different subcategories depending on the mechanistic pathway. For example, for the category of fluorescent probes for anions, we show different types of anions and, furthermore, for different anions, their sites of attack are pointed out. For example, for the CN^- ion, depending on the site of attack, we have categorised them as having (1) the indole moiety as the site of attack by CN^-, (2) the cyanovinyl group as the site of attack by CN^-, and (3) the dicyanovinyl group as the site of attack by CN^-. Our review focuses on a presentation of recent developments of fluorescent probes based on the triphenylamine platform, as published in the literature within the time period 2010–2021. We expect that this literature review will be helpful for the advancement of more potential and exciting fluorescent probes for vast applications in the future.

2 Fluorescent probes based on a triphenylamine platform for anions

Anions, such as cyanide (CN^-),[19] fluoride (F^-)[20] and hypochlorite (OCl^-)[21] play a crucial role in environmental science as well as in medical science and biology.[22] There is a specific limit approved by WHO, known as the permissible limit.[23] Above this permissible limit, CN^- can create various hazardous effects, so it is necessary to develop powerful sensors which can determine the level of this toxic ion. Fluoride, being the smallest anion, possesses distinctive chemical properties, and its detection is critical because it is associated with drinking water analysis, the refinement of uranium used in nuclear weapons manufacture, dental care, and the treatment of osteoporosis.[24,25] Fluorescent sensors for the selective recognition of OCl^- have gained much attention recently, as the excessive deposition of highly oxidative OCl^- inside the human body is injurious and can cause a wide range of diseases.[26,27]

2.1 Triphenylamine derivatives as fluorescent probes for the cyanide ion (CN^-)

2.1.1 Indole moiety as the site of attack by CN^-. In 2015, Wang *et al.* reported a simple conjugated triphenylamine-based probe **1** (Fig. 2) which acts as a cyanide detector.[28] Nucleophilic addition takes places efficiently at its target indolium 2 C atom. So, the cyanide anions can easily bind to it and this interrupts the conjugation between indolium and the triphenylamine moiety, resulting in a turn-off ICT process (Fig. 2) and corresponding spectroscopic changes. The probe shows pH dependence and can act as good CN^- detector in the pH range 5–10. Compound **1** was non-emissive, and upon addition of CN^-, fluorescence was dramatically increased at 445 nm ($\lambda_{ex} = 345$). The detection limit was found to be as low as 21 nM, which indicates the high sensitivity of the probe towards the CN^- ion.

Again, in 2015 Huo's group reported a triphenylamine-based probe **2** (Fig. 2) which is basically a conjugated system between TPA and an indolium group.[29] With the addition of cyanide, probe **2** showed a strong fluorescence emission at 477 nm ($\lambda_{ex} = 345$) based on blocking the ICT process. The mechanism for the 'turn-on' responses was explained as electrophilic addition, which causes inhibition of the ICT process in the probe and this explanation was confirmed by NMR experiments. Basically, probe **2** is an extended form of probe **1**, and the sensing mechanisms are the same for these two probes. Probe **2** was further used to detect CN^- in HepG2 cells, resulting in an outstanding change in fluorescence intensity.

Liu and coworkers reported an NIR probe **3** (Fig. 2) for the selective detection of CN^- ions.[30] In this probe, one indolium

Published on 14 February 2022. Downloaded by Bengal Engineering and Science University on 6/8/2022 1:03:11 PM.

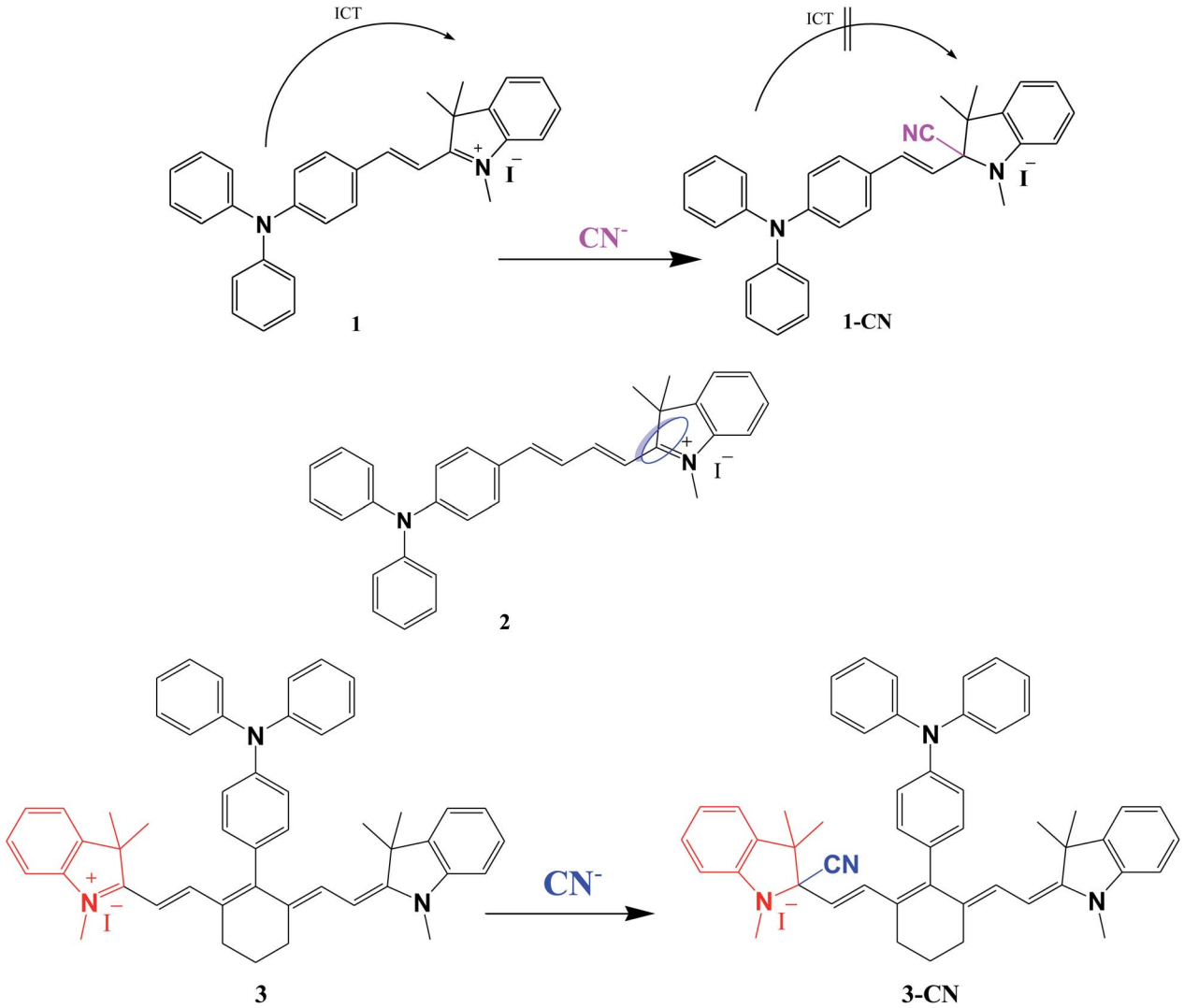

Fig. 2 Structures of probes **1–3** and probable sensing mechanisms of probe **1** and **3** with CN^-.

group and the triphenylamine group act as fluorophores, but the electron-donating group of the indolium salt acts as a site of attack for the CN^- ion. Probe **3** in both CH_3CN and CH_3CN/H_2O (9/1, v/v) exhibits a strong emission peak at 780 nm, which decreases with the gradual addition of CN^- ions. The limit of detection was found to be 14 nM in an acetonitrile solvent system, whereas in a solvent system of acetonitrile–water, the detection limit was found to be 0.23 μM. Later, a biological application was studied using living L929 cells, and CN^- detection was recorded by a fluorescence-off mechanism.

2.1.2 Cyanovinyl group as the site of attack by CN^-. Guan's group developed probe **4** (Fig. 3a) for CN^- detection.[31] Probe **4** showed a distinct naked-eye colour change from dark yellow to colourless and consequently the intensity of fluorescent emission was increased at 565 nm upon the addition of cyanide anions. The pH effect on the fluorescent nature was also examined. From the results it can be concluded that the probe could act as a cyanide detector over a broad range of pH (2 to 12). Mechanistically, nucleophilic attack by CN^- on the vinyl group was assumed, and this assumption was verified and confirmed by ^1H NMR titration and DFT calculations.

Qu's group reported a triphenylamine derivative **5** (Fig. 3b) as a turn-on fluorescent probe, which can detect cyanide in DMF/PBS (1 : 99, v/v) solution.[32] The addition of 4 equivalents of cyanide ions results in a dramatic change in the fluorescence quantum yield from $\Phi_F = 0.124$ to $\Phi_F = 0.314$. The fluorescence emission of compound **5** in pure DMF solution was a weak orange-red fluorescence ($\Phi_F = 0.031$) at 621 nm and with the addition of water the fluorescence decreased with a slight red-shift when f_w (fraction of water vol%) reached 20%. This phenomenon was attributed to an enhancement of the TICT effect of **5**. Interestingly, when the water fraction was increased from 20% to 60%, a clear enhancement in fluorescence was noticed along with an emission band blue-shifted from 626 nm to 565 nm, which indicates the AIE behaviour of the probe. A study of imaging for living organisms *in vivo* was also performed on parts of the heart, spleen, liver, lungs, and kidneys of mice (Fig. 3c).

 This journal is © The Royal Society of Chemistry 2022

Published on 14 February 2022. Downloaded by Bengal Engineering and Science University on 6/8/2022 1:03:11 PM.

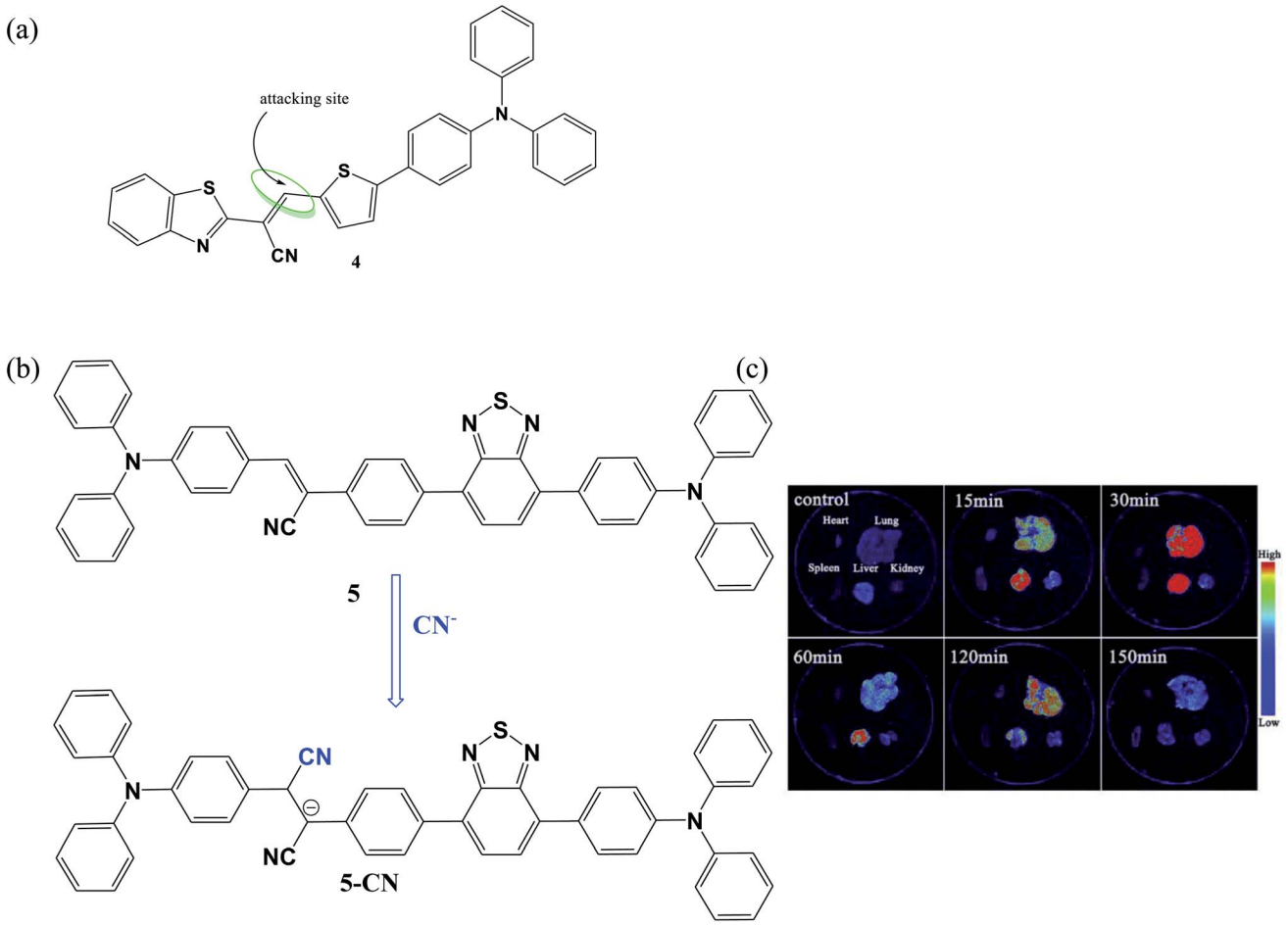

Fig. 3 (a) Structure of probe **4**; (b) reaction of probe **5** with CN^-; (c) fluorescence images of heart, liver, spleen, lung and kidney excised at 0, 15, 30, 60, 120 and 150 min after injected administrations with probe **5**. Reprinted from ref. 32. Copyright (2019), with permission from Elsevier.

2.1.3 Dicyanovinyl group as the site of attack by CN^-. Niamnont's group designed and synthesized a novel phenylacetylene derivative containing a dicyanovinyl group, which is an ICT-based probe **6** (Fig. 4).[33] There was a fluorescence enhancement upon the addition of cyanide. Probe **6** showed an emission band at 460 nm in ACN/H_2O solution (9 : 1 v/v, 10 mM PBS buffer pH = 10.0) with excitation at 368 nm. Upon the addition of CN^-, the emission band centred at 460 nm was increased by changing its fluorescence colour from colourless to greenish blue. The sensing mechanism was explained as nucleophilic attack by CN^- on the probe, converting the quantum efficiency from 0.8% to 200% through blocking of the ICT process (a donor–acceptor system from the amino group of the triphenylamine scaffold to the dicyanovinyl function through π-conjugation).

Siva's group developed a new triphenylamine-based probe **7** (Fig. 4) which exhibits fluorescence enhancement upon the addition of cyanide at a wavelength of 400 nm with excitation at 365 nm.[34] Free probe **7** exhibits moderate fluorescence and, upon the addition of cyanide, the fluorescence changes to strong blue. These changes in spectral data associated with cyanide addition can be attributed to nucleophilic attack by cyanide ions at the β-position of vinyl malononitrile connected to triphenylamine. The detection limit was calculated to be as low as 44 nM, far below the permissible limit suggested by WHO.

Shen and coworkers synthesized probe **8** (Fig. 4) based on triphenylamine and benzothiadiazole.[35] The sensing properties were studied in THF/H_2O solution (99 : 1, v/v). With the gradual addition of CN^- ions, the absorption band at 521 nm decreased and formation of a new band was found at 450 nm. Probe **8** shows emission at 627 nm when excited at 480 nm, with a large Stokes shift of nearly 150 nm. Whereas, upon the addition of other anions F^-, Cl^-, Br^-, NO_2^-, I^-, NO_3^-, $H_2PO_4^-$, HCO_3^-, HS^-, HSO_3^-, SCN^-, NCO^-, SO_3^{2-}, SO_4^{2-}, HPO_4^{2-} and CO_3^{2-}, there was no observable change in the emission spectra. The dicyanovinyl group primarily functions as an acceptor, and after attack by cyanide the conjugation was lost, resulting in corresponding spectral changes. The detection limit of this probe for cyanide was found to be as low as 0.014 μM. The sensing mechanism was confirmed by ^1H NMR titration experiments.

Zhu's group reported an NIR-based probe **9** (Fig. 4) which can recognize CN^- in a colorimetric and fluorometric way.[36] UV-vis absorption and fluorescence spectra of probe **9** were

Published on 14 February 2022. Downloaded by Bengal Engineering and Science University on 6/8/2022 1:03:11 PM.

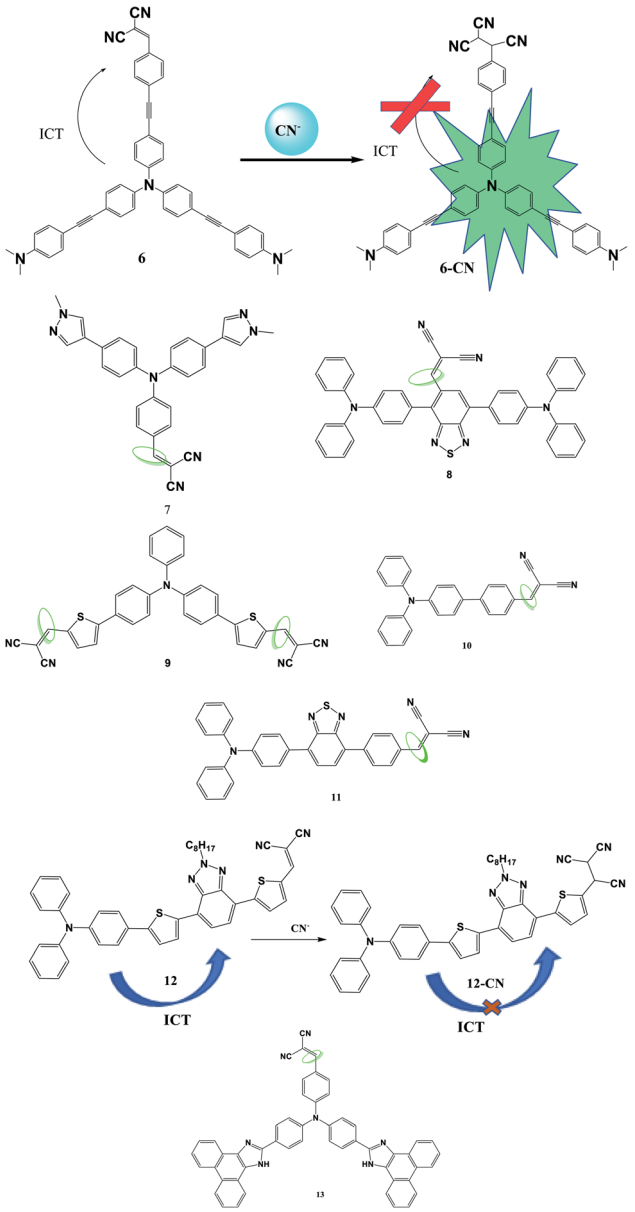

Fig. 4 Structures of probes **6**–**13** and probable sensing mechanism of probes **6** and **12** with CN^-.

measured in THF (5 μM) solution and two absorption bands were noted at 350 nm and 500 nm. The absorption at 350 nm is due to the π–π* transition and the absorption at 500 nm corresponds to the ICT process. The free probe exhibited fluorescence emission at 600 nm corresponding to the NIR emission. Spectral changes upon the addition of different anions were recorded and it was found that there was a dramatic change with the addition of CN^- in the absorption spectrum, but the emission was quenched at 606 nm.

Wu's group designed two triphenylamine-based CN^- probes **10** and **11** (Fig. 4). Probe **10** exhibits 'turn-off' fluorescence, whereas **11** shows 'turn-on' fluorescence in the presence of CN^-.[37] To convert the 'turn-off' response to 'turn-on', the authors increased the electrophilicity of the carbon located at the β position of the dicyanovinyl group and accelerated the reaction with CN^-, by introducing an electron-deficient benzothiadiazole (BTD) group into probe **10** to form probe **11**. Probe **11** was practically applied to detect CN^- in food samples and also in living cells (BEAS-2B cells).

A novel colorimetric fluorescent probe **12** (Fig. 4) with a D–π–A structure for the recognition of CN^- was developed by Huang's group.[38] Probe **12** in THF showed a significant blue-shift of the absorption peak from 514 to 437 nm, which brought about a colour change from amaranth to yellow. Free probe **12** is nonfluorescent, but with the addition of CN^-, a 17-fold fluorescence enhancement at 551 nm was detected and this change was rationalised as the blocking of the ICT process (Fig. 4). Selectivity in the presence of other competing anions was studied, which resulted in good selectivity.

Ozdemir *et al.* designed and synthesized probe **13** (Fig. 4) for cyanide detection by fluorometric enhancement. The mechanism was believed to occur *via* a decrease in the ICT effect caused by the addition of a CN^- ion to the β-carbon of the dicyanovinyl moiety.[39] The limit of detection of the probe was as low as 0.23 μM. The stoichiometric ratio between probe **13** and CN^- was 1 : 1 and the association constant was found to be 5.36 ($\log K_a$).

2.1.4 Other sites of attack by CN^-. In recent years, Ayyanar's group have reported two D–π–D–A-type triphenylamine-based probes **14** and **15** for the recognition of CN^- in 99% aqueous medium (Fig. 5a).[40] Probe **14** alone showed a band of emission at 614 nm. With the addition of CN^-, the band underwent a hypsochromic shift from 614 nm to 574 nm (Fig. 5b). Similarly, probe **15** alone showed a weak band at 604 nm and after the addition of CN^-, a hypsochromic band shift from 604 nm to 564 nm was found. This change was attributed to the interruption of the ICT process from the triphenylamine core to the cyanoacrylic acid receptor. Due to their beautiful spectral changes and low LOD values (234 nM and 11 nM respectively), the probes could be satisfactorily applied for the detection of cyanide in living HeLa cells. So, the dicyanovinyl is not the ultimate acceptor for cyanide detection, and the cyanoacrylic acid receptor is also a good recognition moiety where cyanide addition takes place.

Deng *et al.* designed and synthesized probe **16**, which possesses the so-called AIE property and can selectively detect CN^- (Fig. 5a).[41] The emission intensity located at 581 nm of probe **16** decreased upon the addition of CN^-, which could be accredited to the inhibition of the ICT process. The detection limit of the probe was very low at 2.95×10^{-8} mol L^{-1}. However, the excellent anti-interference property and broad pH range were special features of the probe.

Balamurugan *et al.* reported probe **17** for the selective detection of CN^- *via* an interesting mechanistic pathway (Fig. 5a).[42] The colorimetric and fluorometric changes observed here were attributed to the formation of a new ICT state from the old one, resulting in the disappearance of the absorption band at 425 nm and the generation of a new one at 320 nm, as well as a significant increase in emission at 402 nm. The detection limit was calculated to be as low as 0.36 μM.

 This journal is © The Royal Society of Chemistry 2022

Published on 14 February 2022. Downloaded by Bengal Engineering and Science University on 6/8/2022 1:03:11 PM.

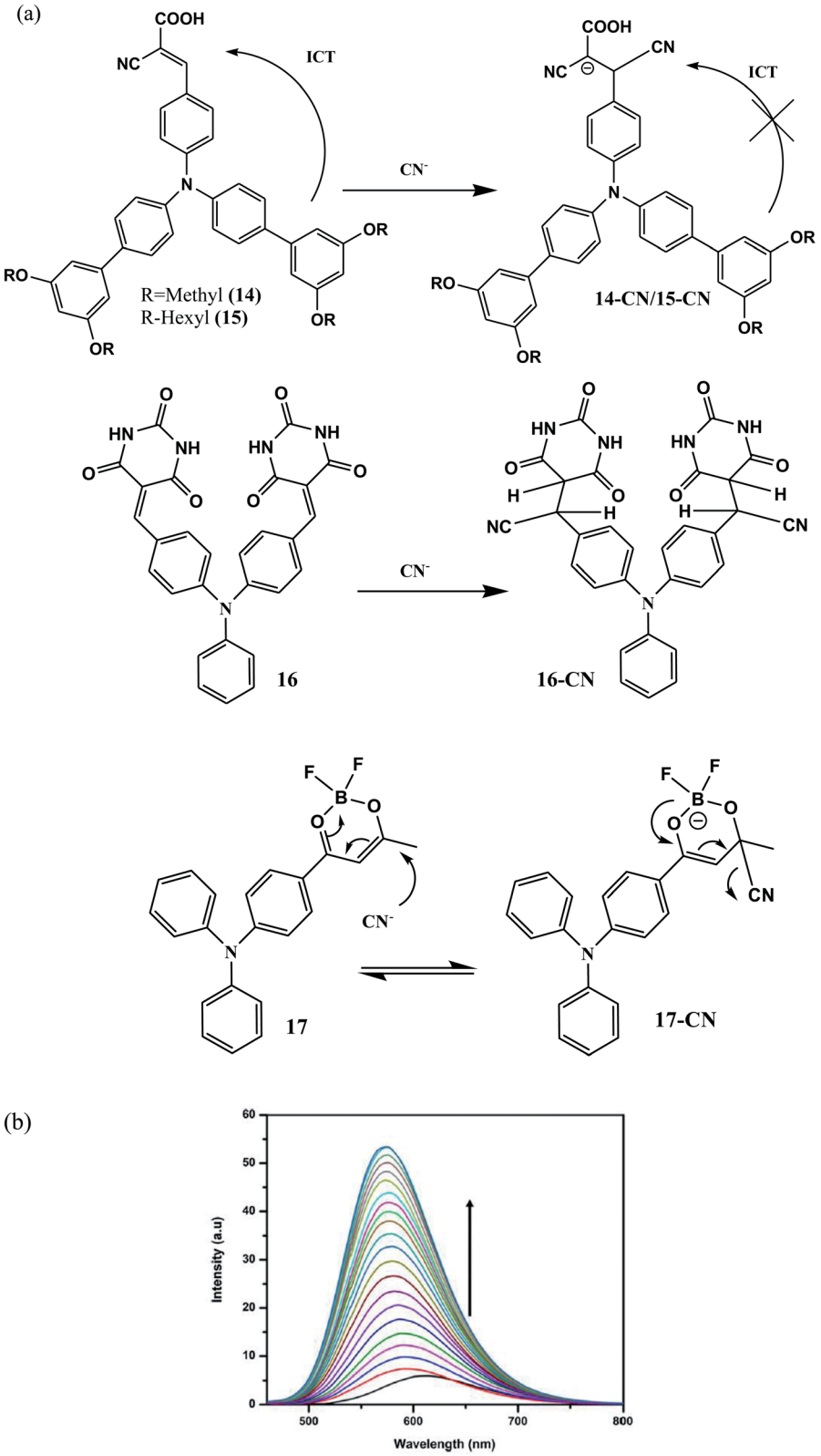

Fig. 5 (a) Structures of probes **14**–**17** and the probable sensing mechanisms of probes **14**–**17** with CN^-. (b) Fluorescence spectra of probe **14** in the presence of different concentrations of CN^- ions. Reprinted from ref. 40. Copyright (2019), with permission from Elsevier.

Published on 14 February 2022. Downloaded by Bengal Engineering and Science University on 6/8/2022 1:03:11 PM.

2.2 Triphenylamine derivatives as fluorescent probes for fluoride ions (F^-)

The mechanism behind F^- sensing by triphenylamine derivatives is the coordination of F^-, which acts as a Lewis base with the hydrogen bond donor of amine and is followed by deprotonation.

Ghosh *et al.* developed two fluorometric probes, **18** and **19** (Fig. 6), for the detection of F^- ions.[43] Probes **18** and **19** both have hydrogen bonding sites for coordination with anions, but probe **18** exhibits better interaction with F^- and shows a better fluorometric response than probe **19**. Probe **18** also interacted with AcO^- and H_2PO_4 and with all three of these ions (F^-, AcO^-, and $H_2PO_4^-$) emission spectra were recorded. In these three cases, the emission was quenched. The better response of **18** over **19** is because of the electron-withdrawing ability of the p-nitro group in **18**, which increases the acidity of the urea proton.

Qu *et al.* developed a novel turn-on florescent probe **20** (Fig. 6) for the selective recognition of F^-.[44] Free probe **20** in acetone shows an emission band at 590 nm and, upon the addition of F^- ions, the band at 590 nm decreased and a new band with a red-shift at 641 appeared through a clear iso-emission point at 616 nm. The ratio of the two intensities at 641 nm and 590 nm ($I_{641\ nm/590\ nm}$) shows a near-linear correlation between 12 and 42 μM, within which the limit of detection of F^- was found to be 4.20 μM in acetone. However, the fluorescence behaviour in acetonitrile was quite different with a sharp increase in the emission band at 631 nm, and the detection limit in acetonitrile was found to be as low as 2.46 μM.

Probes **18–20** act as sensors in the medium of an organic solvent. But F^- ion detection in aqueous media is more desirable in analytical chemistry.

Finally, Padmini's group reported a new probe **21** (Fig. 6) which can detect F^- selectively in aqueous media.[45] A UV-vis study of **21** was undertaken in THF : H_2O (1 : 9, v/v). The free probe exhibits a band at 365 nm and the intensity of the peak increases upon the addition of 10 equivalents of tetrabutylammonium fluoride. With the addition of other anions (Cl^-, Br^-, I^-, CN^-, CH_3COO^-, PO_4^{3-}, $H_2PO_4^-$, SCN^-, $P_2O_7^-$, NO_3^- and NO_2^-), there were no observable changes.

A novel diketopyrrolopyrrole-based luminogen **22** (Fig. 6) was designed and synthesized by Wang's group for the recognition of F^-.[46] Probe **22** showed intense emission at 575 nm in a solution of THF. After the addition of 40 μM F^-, 98% of the emission was quenched. The mechanism of this fluorescence quenching is believed to occur *via* deprotonation by F^-. Again, probe **22** in acetone exhibited weak emission at 579 nm, but after the addition of F^-, this band diminished and a new emission with a blue-shift was found at 487 nm. The compound was further titrated with an ACN solvent system and an interestingly weak emission was found at 547 nm, and upon addition of F^- the fluorescence was quenched at 547 nm and a new blue-shifted emission at 484 nm was observed. The authors explained that these three different behaviours with three different solvent systems are due to the co-existence of interconvertible isomers in solution. A practical application of the detection of water content of commercial products was interestingly presented by the authors.

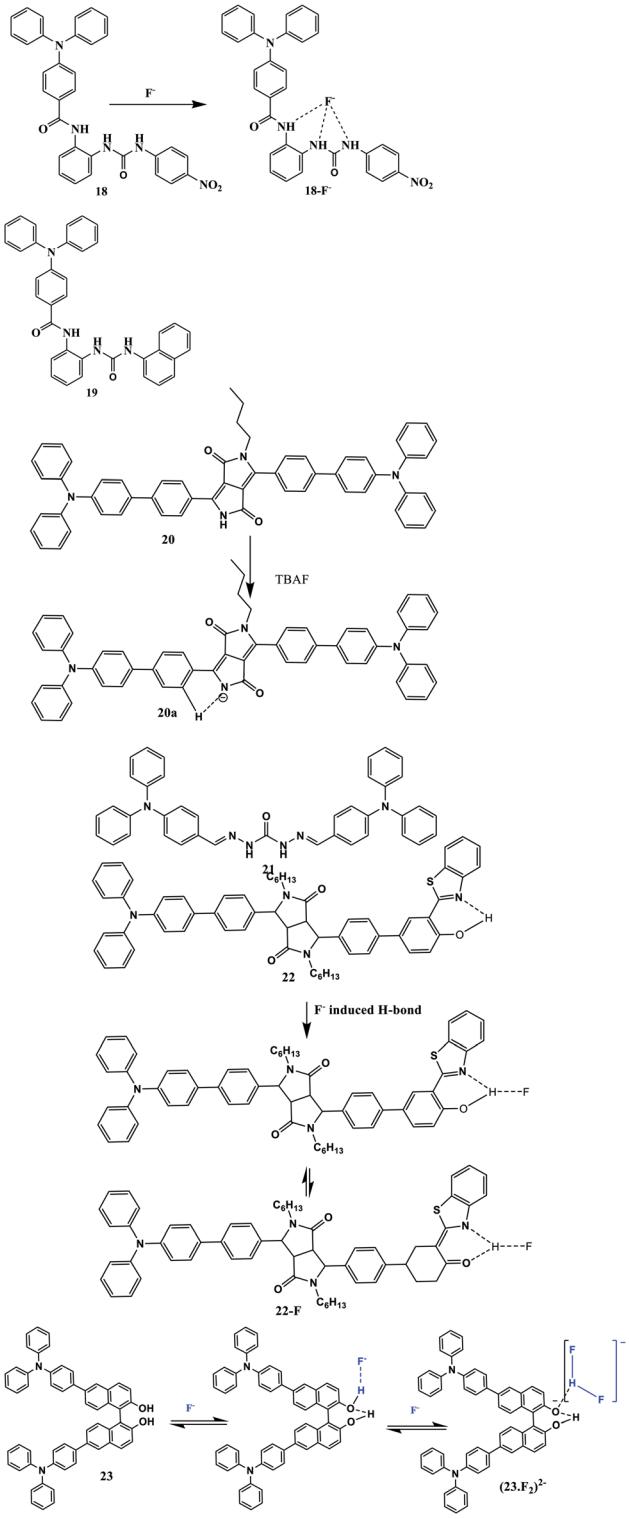

Fig. 6 Structures of probes **18–23** and proposed sensing mechanisms of probes **18**, **20**, **22** and **23** with F^-.

Leung *et al.* designed and synthesized a probe **23** (Fig. 6) which can recognize F^-.[47] Probe **23** in DCM shows fluorescence

 This journal is © The Royal Society of Chemistry 2022

Published on 14 February 2022. Downloaded by Bengal Engineering and Science University on 6/8/2022 1:03:11 PM.

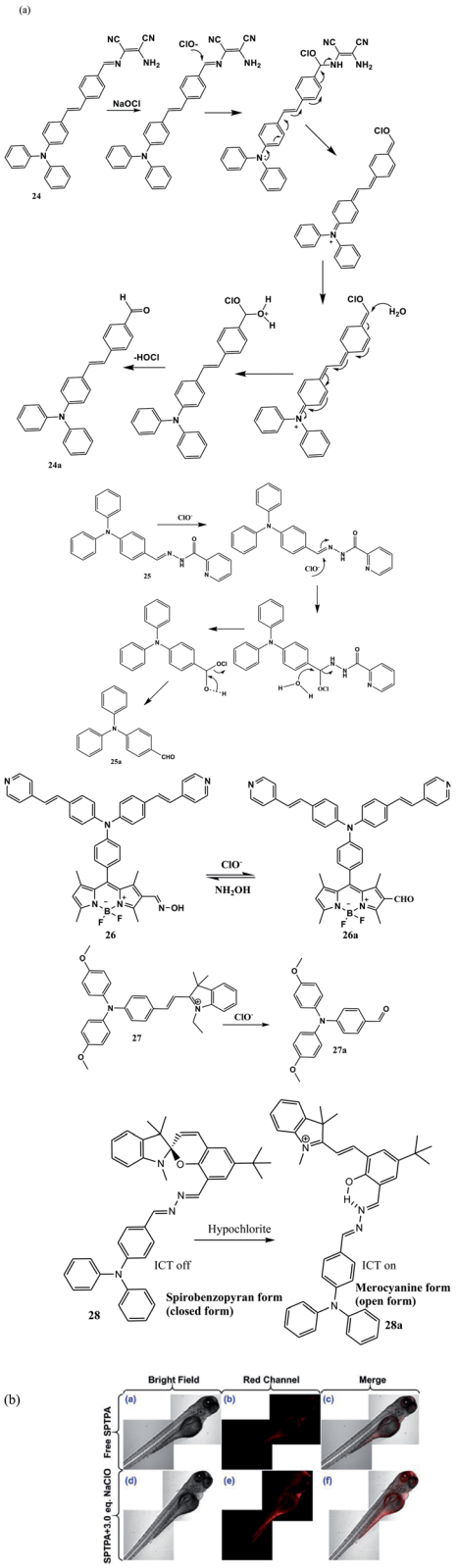

Fig. 7 (a) Structures and probable sensing mechanisms of probes **24**–**28** with hypochlorite. (b) Confocal fluorescence images of zebrafish embryos. (a–c) Fluorescence images of zebrafish stained with probe **28** (2.0 μM) for 20 min. (d–f) Zebrafish were incubated with **28** (2.0 μM) for 20 min, and further incubated with ClO^- (6.0 μM) for 20 min. (a and d) Bright field; (b and e) red channel; (c and f) merged images. Reproduced/Adapted from ref. 54 with permission from The Royal Society of Chemistry.

quenching upon addition of F^-, and this fluorescence quenching experiment was utilized to monitor the binding capacity of the compound. The fluorescence intensity remains almost unchanged with the addition of the first molar equivalents of F^-. However, with the addition of more equivalents of F^-, fluorescence quenching occurs, which indicates 1 : 2 complex formation.

2.3 Triphenylamine derivatives as fluorescent probes for hypochlorite ions (OCl^-)

Hypochlorite is one of the most important ROS in the living body. However, an enormous accumulation of hypochlorous acid/hypochlorite in the human body can cause several severe diseases, such as osteoarthritis, atherosclerosis, rheumatoid arthritis and even cancers.[48,49] So, developing a hypochlorite sensor has great importance. There are several literature studies regarding hypochlorite sensors. Here, we shall discuss only triphenylamine-based sensors for the detection of hypochlorite.

In 2015, Goswami's group developed a diaminomaleonitrile moiety containing a triphenylamine-based fluorescence ratiometric probe **24** (Fig. 7a), which acts as an OCl^- sensor.[50] Probe **24** shows solvatofluorochromism and gives a red-shifted emission band when the solvent changes from non-polar to polar. With excitation at 430 nm, free probe **24** (10 μM, THF/H_2O, 2 : 3, v/v, pH 7.1) exhibits an emission peak at 630 nm. Upon the addition of OCl^- the peak at 630 nm decreased and a new peak at 485 nm appeared. A bioimaging study was also performed with the probe, which showed significant color change in the cells (PBMCs) without an exterior source of OCl^-.

Shen *et al.* reported compound **25** (Fig. 7a) based on a triphenylamine-type Schiff base for the detection of OCl^-.[51] Compound **25** can effectively detect OCl^- in living cells. Probe **25** in aqueous DMSO solution gives two absorption bands around 310 nm and 380 nm, which can be assigned to the triphenylamine and picolinohydrazide moieties, respectively. The probe exhibits fluorescence quenching at 523 nm in the presence of OCl^-, which is caused by breaking of the C=N bond with the formation of raw material upon the addition of OCl^-. Selectivity was also recorded by incorporating various ROS species (50 μM) such as H_2O_2, $^tBuO^-$, HO^-, $^1O_2$, Cl^-, $ONOO^-$,

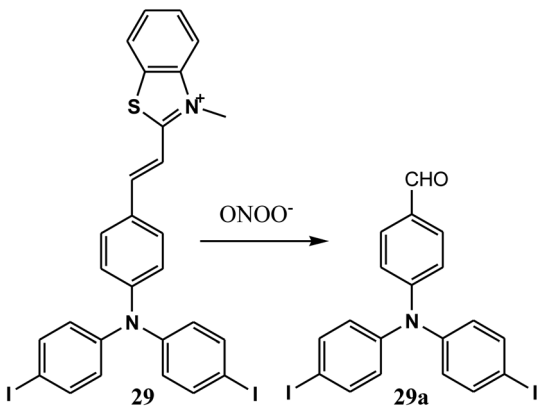

Fig. 8 Structure of probe **29** and its sensing mechanism.

Published on 14 February 2022. Downloaded by Bengal Engineering and Science University on 6/8/2022 1:03:11 PM.

NO_2^-, $H_2PO_4^-$, HCO_3^-, CO_3^{2-} and OCl^-. There was no fluorescence change with the selected ROSs except for OCl^-.

Qian's group designed compound **26** (Fig. 7a) for the colorimetric and fluorometric detection of hypochlorite.[52] Probe **26** contains a BODIPY moiety which adds an attractive feature to the compound. Probe **26** in THF exhibits two absorption bands (393 nm and 520 nm) as well as two emission bands (508 nm and 555 nm). Upon the gradual addition of OCl^- the emission peak increased, both at 508 nm and at 555 nm. With the addition of 50 equivalents of OCl^- with respect to the compound, a 20-fold fluorescence enhancement occurred and the above two peaks merged at 520 nm.

A novel AIE-based fluorescent probe **27** (Fig. 7a) for the easy recognition of ClO^- was further reported by Zhang's group.[53] Within the probe, an indole salt moiety was incorporated to be used as the mitochondria-target and the TPA scaffold was utilised as an AIE active group. Upon addition of ClO^-, oxidation of the ethylene bridge occurred, resulting in a twisted intramolecular charge transfer (TICT) process arising from the donor TPA moiety to the acceptor indole salt moiety. The probe was further used for a practical application to sense ClO^- in living (HeLa) cells.

Chen *et al.* designed and synthesized a chemosensor **28** (Fig. 7a and b) based on spiropyran and triphenylamine, which can recognise ClO^- with high selectivity.[54] Free probe **28** exhibited two sharp absorption peaks at 298 nm and 408 nm, but no emission signal was found with excitation at 408 nm. But after the addition of ClO^-, three absorptions at 298, 371, and 530 nm were noted, and a clear fluorescence enhancement at 605 nm was also observed. The authors rationalised this fluorescence response to 'opening' of the spiropyran ring.

2.4 Triphenylamine derivative as a fluorescent probe for peroxynitrite ($ONOO^-$)

Sun *et al.* designed and synthesized a two-photon fluorescent molecule **29** (Fig. 8).[55] Probe **29** exhibits high sensitivity to $ONOO^-$ in water/glycerol (2/3) solvent and also shows high selectivity over other ROSs. **29** was a triphenylamine-based two-photon fluorescent probe which was reported first as possessing organelle-targeting viscosity quantitation properties and also possessing the ability to detect $ONOO^-$ in mitochondria. The probe exhibits two emission peaks at 407 nm due to local emission and at 647 nm due to the TICT (twisted intramolecular charge transfer) transition. After the addition of $ONOO^-$, the peak at 650 nm decreased with appearance of a new emission band at 485 nm.

3 Fluorescent probes based on a triphenylamine platform for metal ions

A variety of metal ions, such as Cu^{2+}, Al^{3+}, Mg^{2+}, Fe^{3+}, and Zn^{2+}, play important roles in living organisms, but excessive or insufficient amounts can cause a variety of diseases.[56–67] For instance, copper plays a vital role in various biological processes. However, Cu^{2+} has a good redox property and can cause different health issues by accelerating the production of reactive oxygen species (ROSs). There is a tolerable range of concentrations of Cu^{2+}, but concentrations above or below this range can lead to a number of diseases: for example, Alzheimer's disease, Parkinson's disease, hypoglycaemia, outpatient diseases and fatty liver. Some heavy metal ions, including Hg^{2+} and Pb^{2+}, have been used widely in industrial processes. They are highly toxic, even at a minor scale, so the detection of these ions has great importance in environmental sciences.

3.1 Triphenylamine derivatives as fluorescent probes for Cu^{2+}

Xie and co-workers reported compound **30** (Fig. 9) for the selective and sensitive detection of Cu^{2+}.[68] Probe **30** itself had no fluorescence due to PET and C=N isomerisation. In the presence of Cu^{2+} a strong fluorescence was noted due to PET inhibition and inhibition of C=N isomerisation. The free probe showed an absorption band at 380 nm in CH_3CN and at 382 nm in CH_3CN/H_2O (v/v = 4/6, pH = 7.4) HEPES buffer solution. Upon the addition of Cu^{2+}, both the absorbance at 380 nm in CH_3CN and at 382 nm in aqueous acetonitrile solution decreased, and new peaks appeared at 358 nm and 360 nm, respectively. The fluorescence response was interesting. Fluorescence intensity was maximized upon the addition of 2.67 equivalents of Cu^{2+} in 10 μM CH_3CN and 1.5 equivalents of Cu^{2+} in CH_3CN/H_2O (v/v = 4/6, pH = 7.4) HEPES buffer, respectively. The stoichiometry of the complex was determined to be a 1 : 1 complex, as depicted in Fig. 9.

Mahapatra *et al.* developed a TPA-based Cu^{2+} sensor **31** (Fig. 9).[69] Probe **31** in CH_3CN/H_2O (70/30, v/v) solution only sensed Cu^{2+} among heavy and transition metals (HTM). When Cu^{2+} gets captured by the receptor unit of the compound, deprotonation of the secondary amine occurs and the electron-donation ability is enhanced, which results in a change in absorption from 291 nm to 541 nm to give a colorimetric response. However, fluorescence quenching is observed at 378 nm with the addition of Cu^{2+}. The stoichiometric relation between probe and metal was determined to be 1 : 2 complex formation.

In 2020, Chen *et al.* reported Cu^{2+}-sensitive probe **32** (Fig. 9). Probe **32** in aqueous DMSO showed two absorption peaks at 298 nm and 372 nm.[70] Interestingly, the absorbance peak at 372 nm increased and the peaks at 298 nm decreased upon the gradual addition of Cu^{2+}, indicating coordination of probe **32** with the metal and the stoichiometry was reported as 2 : 1 between **32** and Cu^{2+}. With the addition of 0.5 equivalents of Cu^{2+}, a red-shifted absorption was noted, which could be attributed to metal to ligand charge transfer (MLCT). The compound exhibited intense fluorescence emission with λ_{max} = 476 nm, which was due to blocking the intramolecular charge transfer (ICT).

Zhou's group reported a triphenylamine–isophorone based compound **33** (Fig. 9) to detect Cu^{2+} colorimetrically and fluorometrically.[71] For probe **33** in acetonitrile, with the addition of Cu^{2+} (1 equiv.), the absorption band at 417 nm disappeared and the fluorescence intensity increased by eight times at 637 nm.

 This journal is © The Royal Society of Chemistry 2022

Published on 14 February 2022. Downloaded by Bengal Engineering and Science University on 6/8/2022 1:03:11 PM.

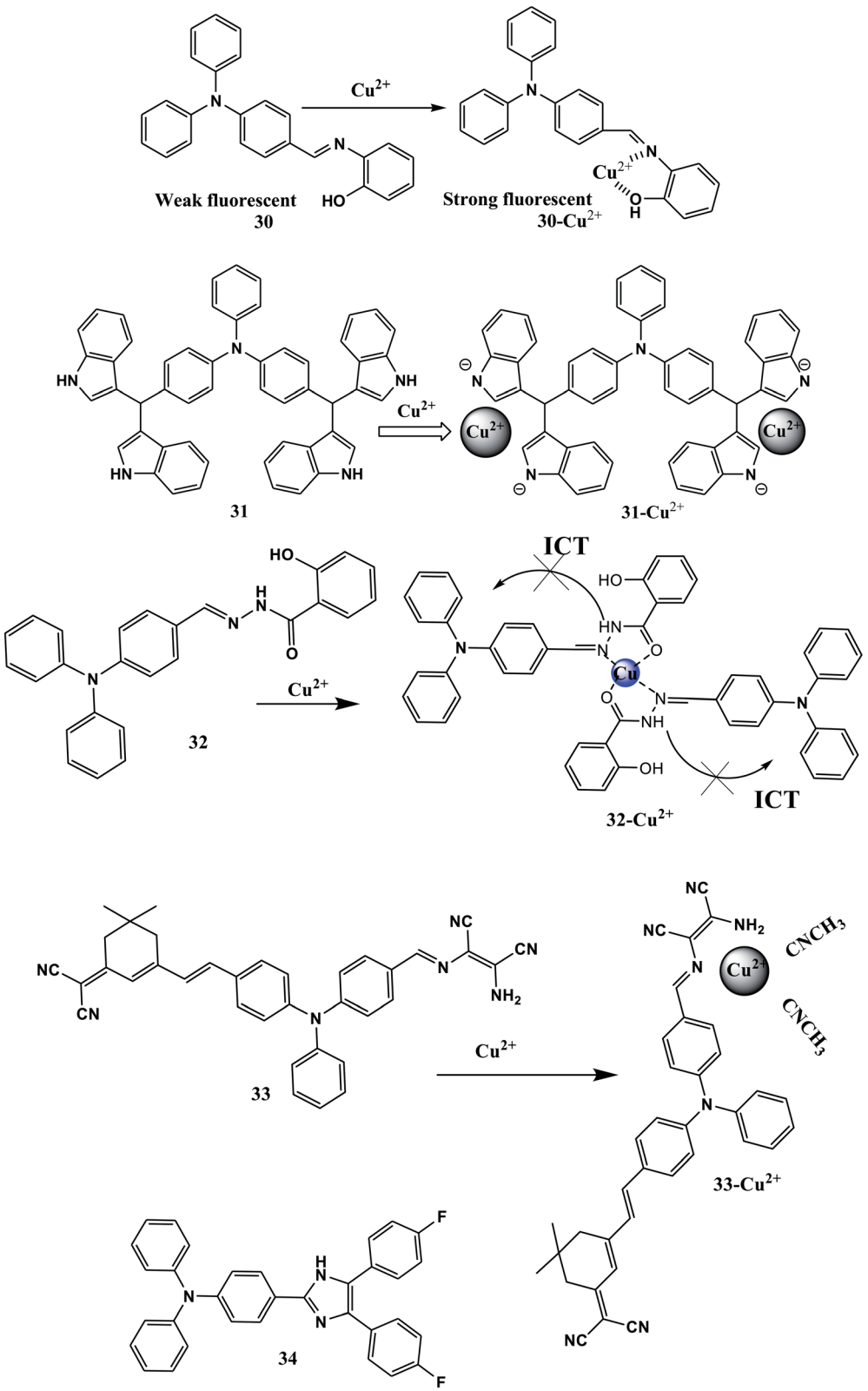

Fig. 9 Structures of probes 30–34 and proposed sensing mechanisms of probes 30–33 with Cu^{2+}.

The detection limit of the compound was calculated as 1.568×10^{-6} M for Cu^{2+}. The compound was very selective towards Cu^{2+} over other competitive metal ions.

In recent years, Wang's group reported triphenylamine-based probe **34**, which can recognize Cu^{2+} in a selective manner (Fig. 9).[72] With the incorporation of Cu^{2+}, the

Published on 14 February 2022. Downloaded by Bengal Engineering and Science University on 6/8/2022 1:03:11 PM.

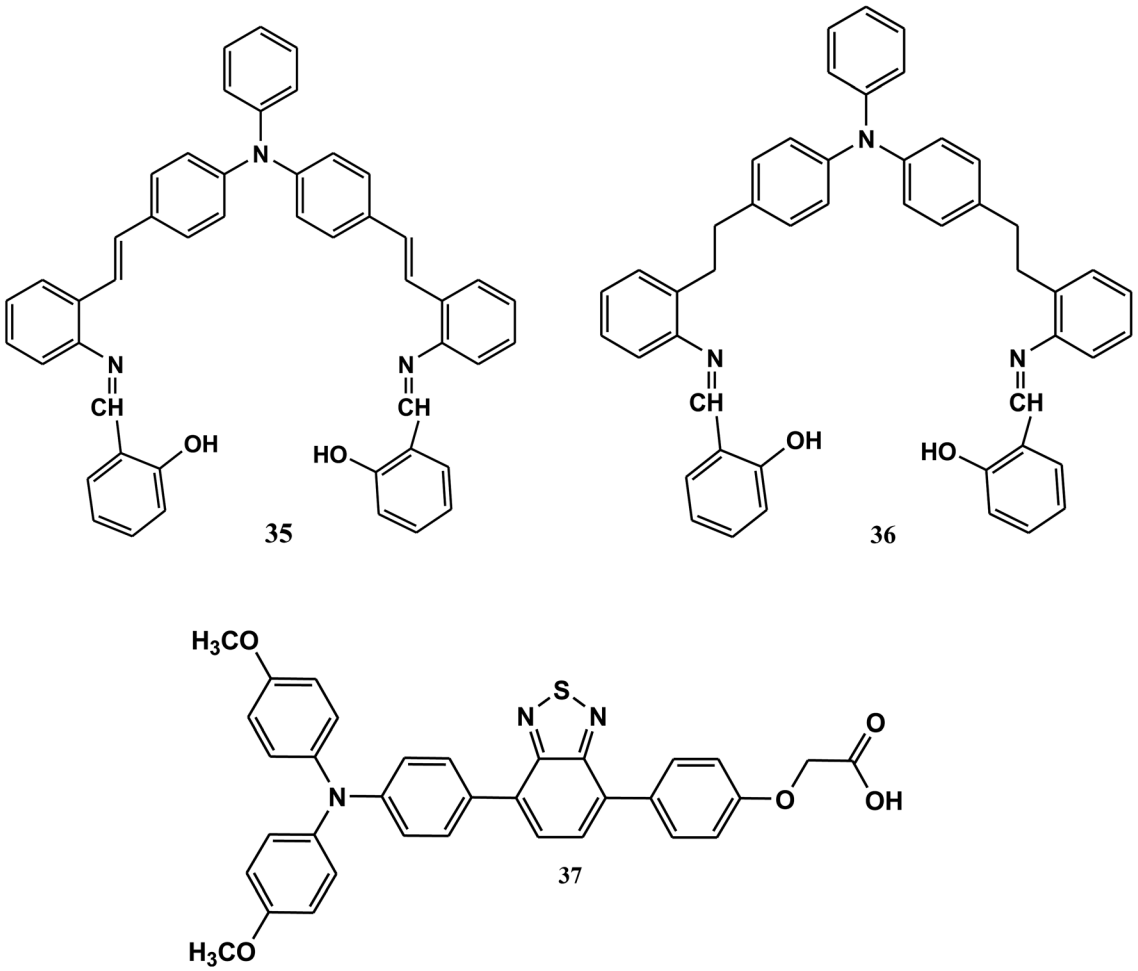

Fig. 10 Structures of probes **35–37**.

absorption of probe **33** at 348 nm decreased and a new absorption peak at 575 nm was generated. At the same time, fluorescence emission gradually decreased at 408 nm with a quenching ratio of 99.82%. The authors showed the formation of a 1 : 1 complex between the probe and Cu^{2+} in a Job plot.

3.2 Triphenylamine-based derivatives as fluorescent probes for Al^{3+}

Gan *et al.* reported two triphenylamine-based Schiff bases **35** and **36** (Fig. 10) for the detection of Al^{3+}.[73] The selectivity was studied with a wide range of metal ions (Cu^{2+}, Hg^{2+}, Zn^{2+}, Mg^{2+}, Pb^{2+}, Ca^{2+}, Cd^{2+}, Ag^{+}, Ni^{2+}, Mn^{2+}, Co^{2+}, Li^{+}, K^{+}, Na^{+}, Ni^{2+}, Ba^{2+}, Ce^{2+}, Al^{3+}, Cr^{3+} and Fe^{3+}). Probe **35** exhibited a 6-fold enhancement in fluorescence in the presence of Al^{3+} at 481 nm, and a small, negligible, fluorescence change was also observed for Cr^{3+} and Fe^{3+}. However, probe **36** exhibited selective 20-fold fluorescence enhancement with the gradual addition of Al^{3+} at 513 nm. Surprisingly when **35** was titrated with Al^{3+} a red-shifted fluorescence emission from 450 nm to 489 nm was observed.

Hua's group developed a fluorescent turn-on probe **37** (Fig. 10) based on a dimethoxy triphenylamine benzothiadiazole derivative.[74] Free probe **37** exhibited AIE behaviour. Probe **37** in a DMSO/HEPES mixture (containing 50 vol% DMSO, pH = 7.0) was nearly non-emissive in the absence of Al^{3+}. However, with the incorporation of Al^{3+}, the intensity of fluorescence emission at 580 nm increased by more than 10 times. The compound showed selectivity with a detection limit of 1.5×10^{-7} M. Further detection of Al^{3+} in living HeLa cells in fish was performed and strong red fluorescence was observed.

3.3 Triphenylamine derivatives as fluorescent probes for Fe^{3+}

Pan *et al.* reported **38** (Fig. 11a) for the detection of Fe^{3+} by a turn-off method.[75] Interestingly, the compound shows AIE behaviour in the free environment, but shows fluorescence-off behaviour with the incorporation of Fe^{3+}. The mechanism involved here is PET through the formation of a stoichiometric 2 : 1 complex. The limit of detection was found to be as low as 4.51×10^{-5} M. Further biological imaging and membrane permeability show that the probe can also detect Fe^{3+} in living cells.

 This journal is © The Royal Society of Chemistry 2022

Published on 14 February 2022. Downloaded by Bengal Engineering and Science University on 6/8/2022 1:03:11 PM.

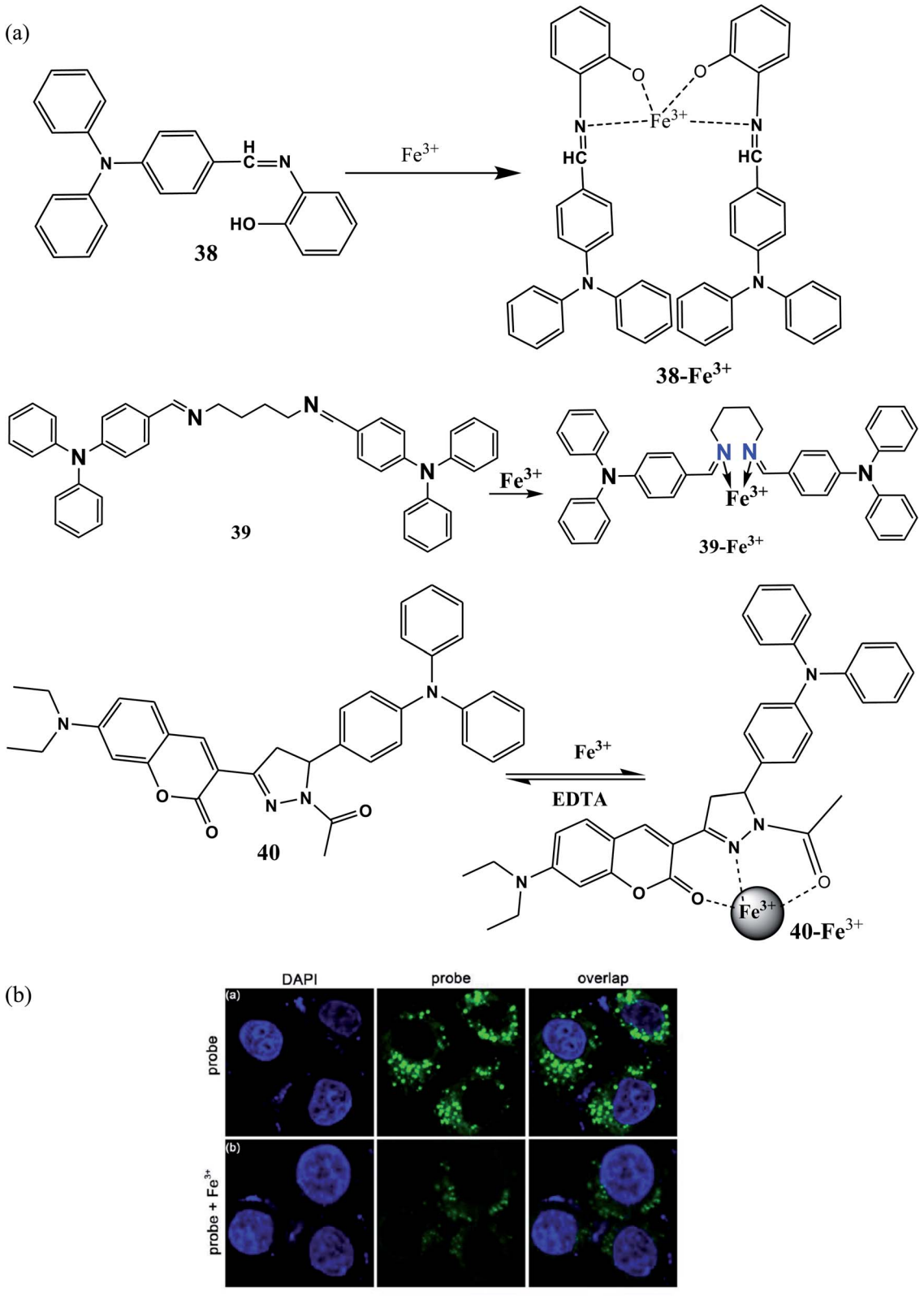

Fig. 11 (a) Structures of probes **38–40** and probable sensing mechanisms of probes **38–40** with Fe^{3+}. (b) Fluorescent imaging of HeLa cells treated with (a) only probe **39** (5 μM) and (b) after the addition of Fe^{3+} ions (20 μM). Reprinted from ref. 76. Copyright (2016), with permission from Elsevier.

Published on 14 February 2022. Downloaded by Bengal Engineering and Science University on 6/8/2022 1:03:11 PM.

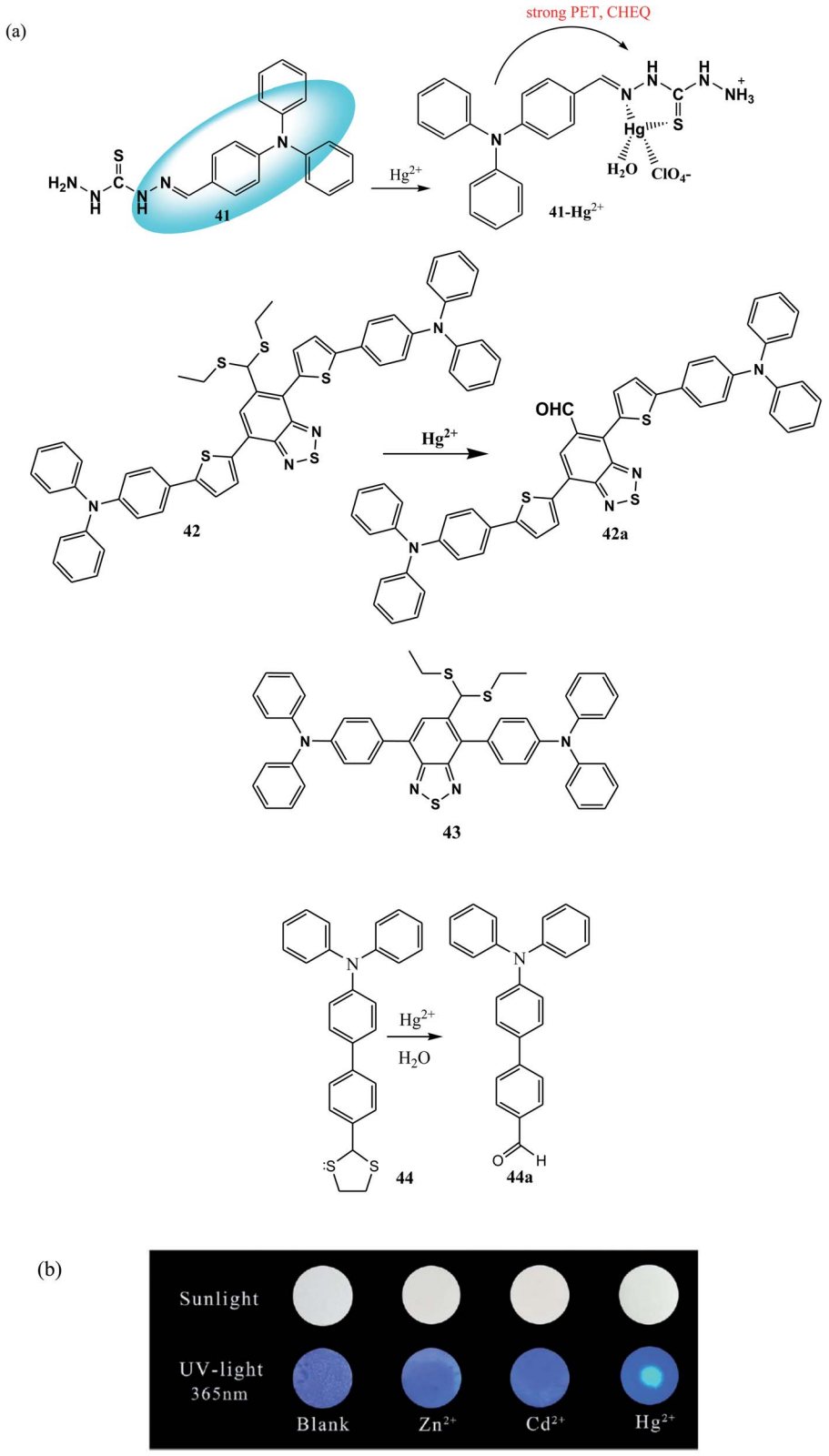

Fig. 12 (a) Structures of probes **41**–**44** and probable sensing processes of probes **41**, **42** and **44**. (b) Photographs of **44**-based test paper. Reproduced/Adapted from ref. 81 with permission from The Royal Society of Chemistry.

Qu *et al.* designed and synthesized **39** (Fig. 11a), which can recognize Fe^{3+} in aqueous media.[76] The probe exhibits blue fluorescence in aqueous solution, and the fluorescence quenches upon the addition of Fe^{3+} to the solution. The scenario behind the fluorescence quenching is the intramolecular charge transfer (ICT) or energy transfer process from

 This journal is © The Royal Society of Chemistry 2022

Published on 14 February 2022. Downloaded by Bengal Engineering and Science University on 6/8/2022 1:03:11 PM.

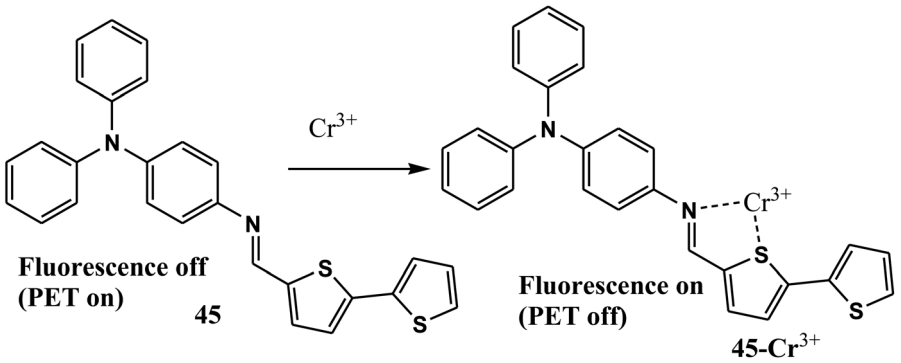

Fig. 13 Structure of probe **45** and its sensing mechanism.

triphenylamine to butanediamine promoted by coordination interaction. The authors also explored cell imaging studies using HeLa cells and explained the Fe^{3+} detection (Fig. 11b).

Zhang *et al.* reported probe **40**, for the selective detection of Fe^{3+} by turn-off fluorescence (Fig. 11a).[77] Probe **40** in THF showed an intense emission band located at 523 nm (quantum yield = 0.326), but with the incorporation of Fe^{3+}, the intensity of the fluorescence decreased to 45% (quantum yield = 0.108). The authors demonstrated that the carbonyl group of benzopyrone in probe **40**, CH=N, and C=O on the pyrazole ring were involved in the coordination of Fe^{3+} in a 1 : 1 mode using infrared titration and DFT.

3.4 Triphenylamine derivatives as fluorescent probes for Hg^{2+}

Compounds **41–43** (Fig. 12a) are all furnished with recognition centres which can accommodate Hg^{2+} in a selective manner and their fluorescence behaviours were further investigated based on the coordination mechanism.

Li *et al.* reported a mono-aromatic-aldehyde-thiosemicarbazones-based probe (Fig. 12a).[78] Probe **41** in DMSO/Tris–HCl (8/2, v/v) showed fluorescence quenching upon the addition of Hg^{2+}, followed by a red-shift of the absorption spectrum. The limit of detection was set at 3.11×10^{-8} M. The mechanism involved was strong PET upon complex formation. The probe was further utilised to detect Hg^{2+} in real water samples and was also applied for biological detection.

Shen's group reported an NIR ratiometric fluorescent probe **42**, which can detect Hg^{2+} by a desulfurisation mechanism (Fig. 12a).[79] This compound was synthesized by the strategy of extended π-conjugation between triphenylamine and benzothiadiazole. To investigate the selectivity, excess amounts of metal ion salts (2 equiv.) of K^+, Na^+, Ag^+, Co^{2+}, Mn^{2+}, Zn^{2+}, Ca^{2+}, Pb^{2+}, Ni^{2+}, Mg^{2+}, Cu^{2+}, Cr^{3+}, Al^{3+} and Fe^{3+} were incorporated into compound **42**. However, only Hg^{2+} exhibited a bathochromic shift in the UV-vis absorbance from 489 nm to 535 nm under the same conditions, which indicates the high selectivity for Hg^{2+}.

Again, Shen's group developed **43** for the selective detection of Hg^{2+} by a desulfurisation mechanism (Fig. 12a).[80] Probe **43** in THF–water (99 : 1) solution gives an absorption maximum at wavelength 438 nm and an emission maximum at wavelength 600 nm. Interestingly, the protected aldehyde group reverts back to the original aldehyde with the addition of Hg^{2+}, and the D–A–D structure is converted into a D–A–A structure. Therefore, the degree of ICT increases and results in an amazing red-shift of the absorption and also the fluorescence bands of the sensor. As a result, the fluorescence changes from 600 nm to 650 nm and the naked-eye color changes from yellow to red.

Probe **44** is an example of the traditional aggregation-induced emission (AIE) class of fluorophores (Fig. 12a and b).[81] Probe **44** in DMF/H_2O (f_w 70%, pH 6.8) showed an emission band at 451 nm, which was shifted to 462 nm upon the addition of Hg^{2+}. Selectivity was also tested, but no interference was found. The limit of detection of the probe was as low as 1.23×10^{-7} mol L^{-1}.

3.5 Triphenylamine derivative as a fluorescent probe for Cr^{3+}

Kaya's group developed a new Schiff base **45** (Fig. 13) to detect Cr^{3+}.[82] Free **45** showed no fluorescence. Upon the addition of Cr^{3+} to a solution of THF, a 59-fold fluorescence enhancement was observed at 471 nm. The mechanism behind this fluorescence change involves PET quenching. In **45** the PET process was observed where triphenylamine acts as a donor and thiophene units as acceptors through the π linker of C=N. With the addition of Cr^{3+}, chelation occurred between Cr^{3+}, S and N, leading to interruption in the PET process and consequently enhancement in the fluorescence was observed.

3.6 Triphenylamine derivative as a fluorescent probe for Sn^{2+}

Kolcu *et al.* designed and synthesized a triphenylamine-based probe **46** which can recognize Sn^{2+} by a potent chelation enhanced fluorescence (CHEF) effect.[83] Probe **46** showed no fluorescence because of PET and C=N isomerisation, but in the presence of Sn^{2+}, the CHEF effect leads to restriction of the electron transfer process, resulting in fluorescence emission at 460 nm. The authors proved that Sn^{2+} ions were bound to **46** in 2 : 1 (metal : ligand) stoichiometry and also calculated that the fluorescence quantum yield of **46** in the presence of Sn^{2+} was 24% (Fig. 14).

Published on 14 February 2022. Downloaded by Bengal Engineering and Science University on 6/8/2022 1:03:11 PM.

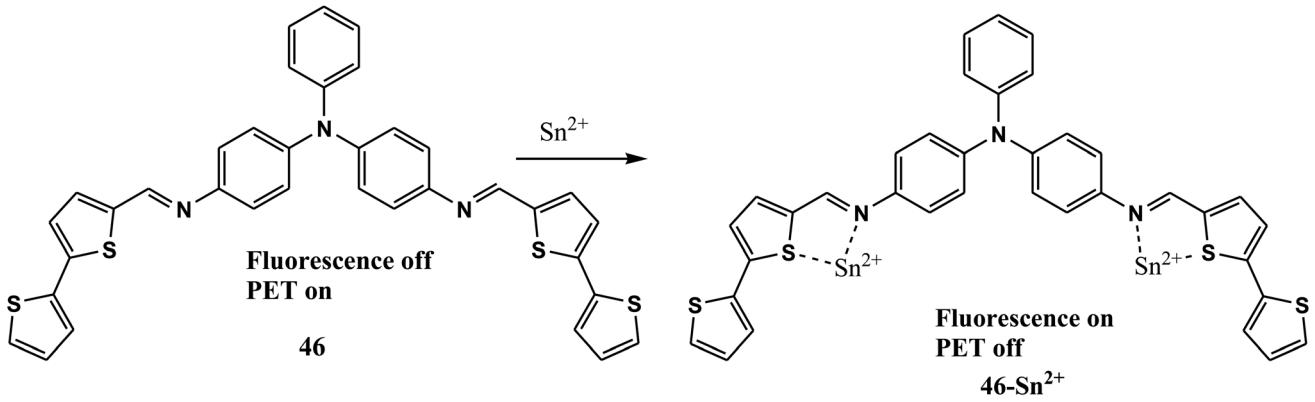

Fig. 14 Structure of probe **46** and its probable sensing mechanism.

3.7 Triphenylamine derivatives as fluorescent probes for dual/multiple ions

Although the above-mentioned sensors have selectivity towards a specific ion, there are several sensors which can detect two or more ions simultaneously.

The triphenylamine–aminonaphthol conjugate **47** (Fig. 15) can selectively recognise Zn^{2+} and Cd^{2+} *via* complex formation.[84] The fluorescence enhancement was 10-fold for Zn^{2+} and 8-fold for Cd^{2+}. The detection limit was found to be $(3.43 \pm 0.21) \times 10^{-6}$ M for Cd^{2+} and $(3.16 \pm 0.18) \times 10^{-6}$ M for Zn^{2+}. The mechanism was believed to occur *via* the coordination of Schiff-base derivative **47** to Cd^{2+} and Zn^{2+}. This coordination inhibits C=N isomerization as well as the ICT process, resulting in increased fluorescence.

Two triphenylamine-based probes **48** and **49** (Fig. 15) were designed to recognise multiple ions.[85] With the addition of Zn^{2+}, both probes showed turn-on fluorescence with a 36-fold (λ_{max} = 488 nm) increment, but upon the addition of Cd^{2+} to a mixture of probe and Zn^{2+}, a ratiometric fluorescence change was observed and the fluorescence increased by 190-fold (λ_{max} = 466 nm). However, both probes can detect Mn^{2+} by a colorimetric change observable by the naked eye.

Yang *et al.* reported two triphenylamine-based dyes, **50** and **51** (Fig. 15).[86] Probe **50** in acetonitrile can recognise Fe^{3+} and Hg^{2+} through 1 : 1 complex formation, which interrupts the PET process and results in quenching of fluorescence. At 436 nm, probe **51** exhibits efficient and stable amplified spontaneous emissions (ASE).

Malkondu's group reported compound **52** (Fig. 15) as a dual sensor for Hg^{2+} and Cu^{2+}.[87] But the detection of Hg^{2+} is colorimetric, whereas the detection of Cu^{2+} is fluorometric in nature. **43** in aqueous ACN showed three absorption bands at 271 nm, 340 nm, 370 nm, which could be attributed to π–π* transitions for the first two bands, and an n–π* transition for the third band. After the addition of 5 equivalents of Hg^{2+}, a naked-eye color change was observed from colorless to yellow. Dramatically, there was a slight quenching in emission with the addition of Hg^{2+}, but enhanced emission was found in the case of Cu^{2+}.

Ziqiwang *et al.* developed probe **53** (Fig. 15) for detection of both Fe^{3+} and Cu^{2+}.[88] A fluorescence study of **53** in ACN solution showed that the fluorescence emission intensity decreased when Fe^{3+} and Cu^{2+} solutions were added to the probe solution. The detection limits of Fe^{3+} and Cu^{2+} with **53** were 230 nM and 620 nM, respectively. The emissive property study revealed that the fluorescence quantum yields of **53**, and **53**-Fe^{3+} and **53**-Cu^{2+} complexes are 41%, 0.6% and 1.5%, respectively. From the absorption spectrum, it is obvious that the electron-donating ability of the probe is decreased by coordination with Fe^{3+}/Cu^{2+}, which results in red-shifted absorption.

Both compounds **54** and **55** (Fig. 15) can detect Al^{3+} and Fe^{3+} through decolorisation from a yellow color, through the mechanism of hydrolysis in the presence of Lewis–acidic Fe^{3+} and Al^{3+} and transformation to the corresponding amine and aldehyde.[89] For both compounds, the rate of decolorisation was the same in the solvent acetonitrile. But the rate of decolorisation was different in the solvent DMF. Again, the distinguishable properties for the compounds were found in the fluorometric response. However, probe **55** also exhibited a fluorescence turn-on response upon treatment with Zn^{2+} in DMF. The enhanced fluorescence was due to the restriction of C=N isomerization *via* metal coordination.

Shu's group reported compound **56** (Fig. 15) to recognize Zn^{2+} and CN^-.[90] With the incorporation of Zn^{2+}, the compound exhibited fluorescence enhancement because binding with Zn^{2+} in 1 : 3 stoichiometry causes the chelation-enhanced fluorescence emission (CHEF) effect and inhibits C=N isomerisation. However, in the presence of CN^-, continuous emission quenching at 565 nm was observed. From ^{1}H NMR experiments, it was proved that the fluorescence quenching occurs due to loss of conjugation after the addition of cyanide to the probe.

Erdemir designed a novel triphenylamine-conjugated rhodamine derivative **57** (Fig. 15) to detect cations.[91] Probe **57** in MeCN/H_2O (v/v, 9/1) showed high selectivity for Hg^{2+} and Al^{3+} ions *via* two completely different sensing mechanisms. For example, Hg^{2+} ion sensing was due to spirolactam ring-opening in rhodamine and Al^{3+} ion sensing was due to the PET process in the triphenylamine moiety. The Hg^{2+} and Al^{3+} ions

 This journal is © The Royal Society of Chemistry 2022

Published on 14 February 2022. Downloaded by Bengal Engineering and Science University on 6/8/2022 1:03:11 PM.

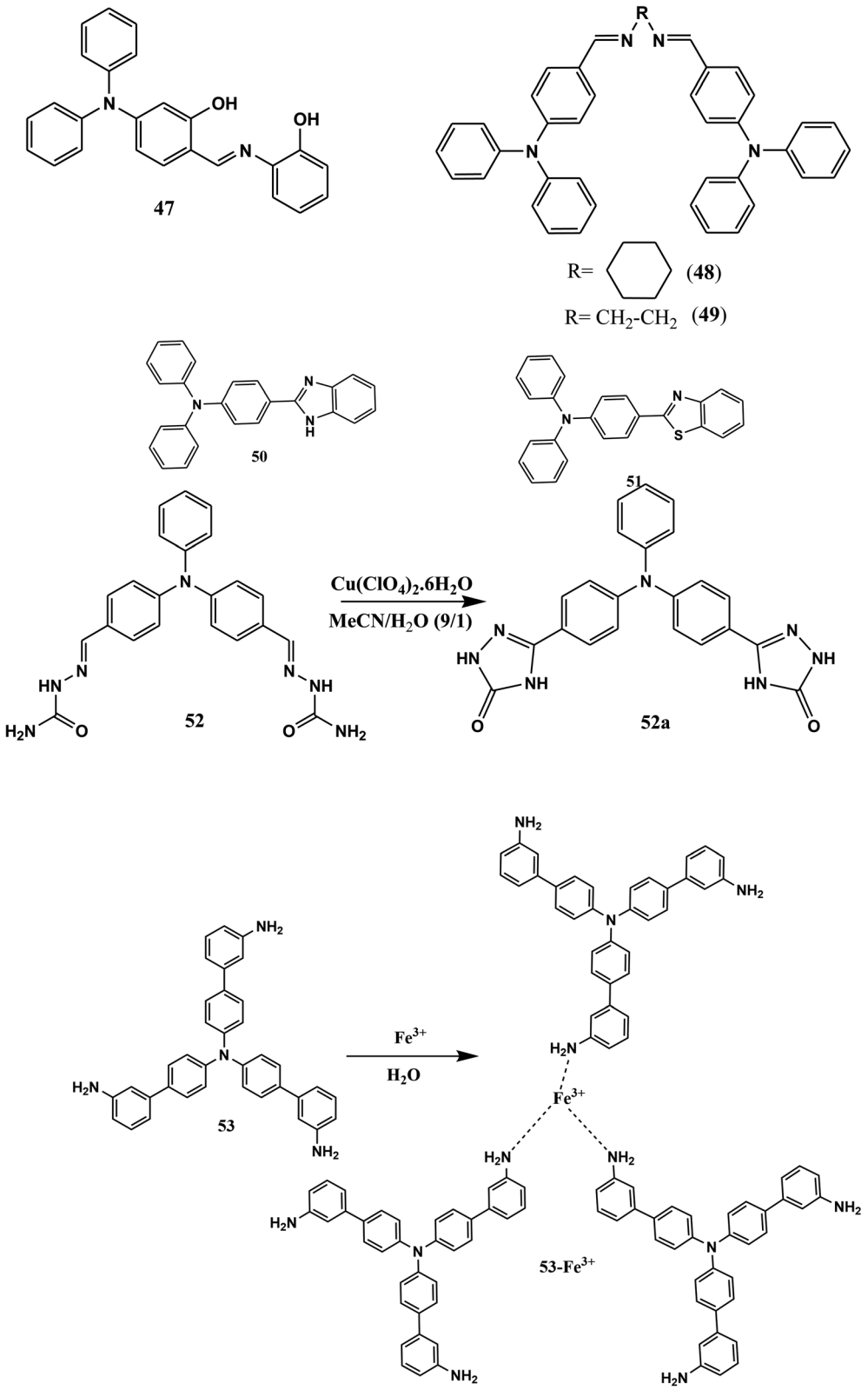

Fig. 15 Structures of probes 47–60 and probable sensing processes of probes 52, 53, 56, 57 and 58.

Published on 14 February 2022. Downloaded by Bengal Engineering and Science University on 6/8/2022 1:03:11 PM.

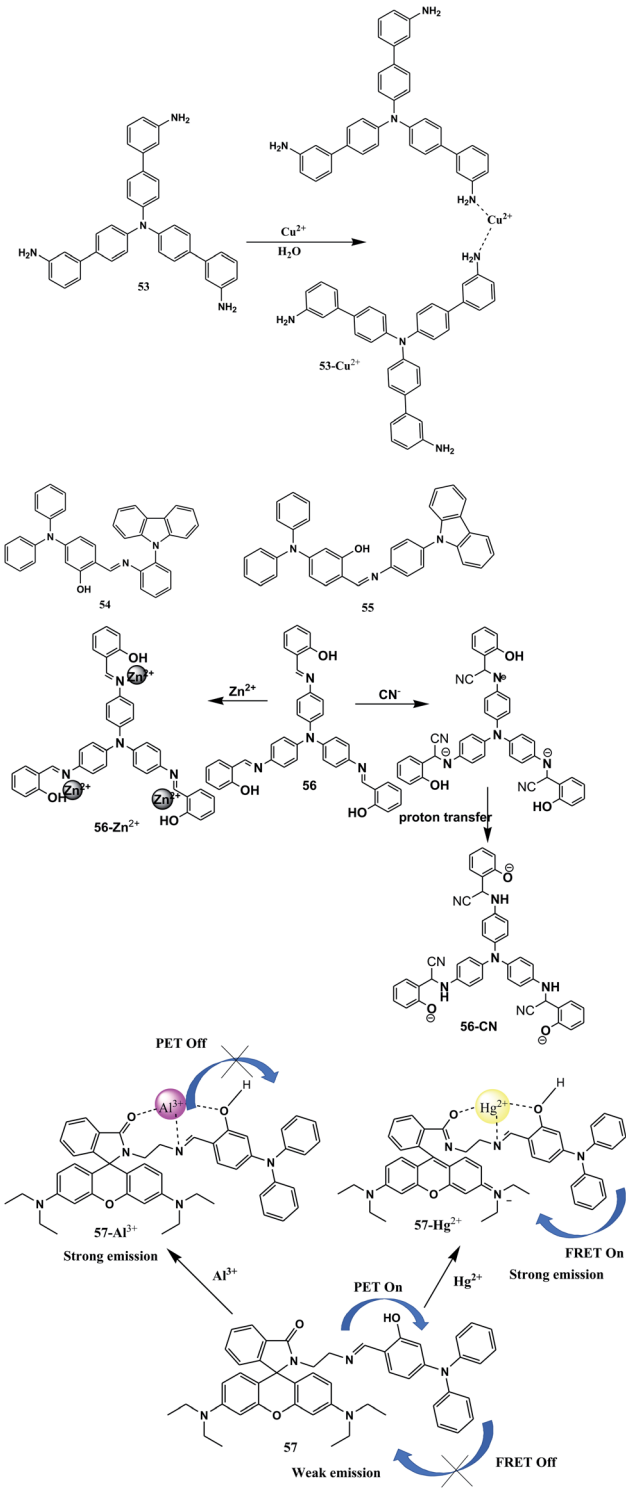

Fig. 15 (*contd.*)

This journal is © The Royal Society of Chemistry 2022

Published on 14 February 2022. Downloaded by Bengal Engineering and Science University on 6/8/2022 1:03:11 PM.

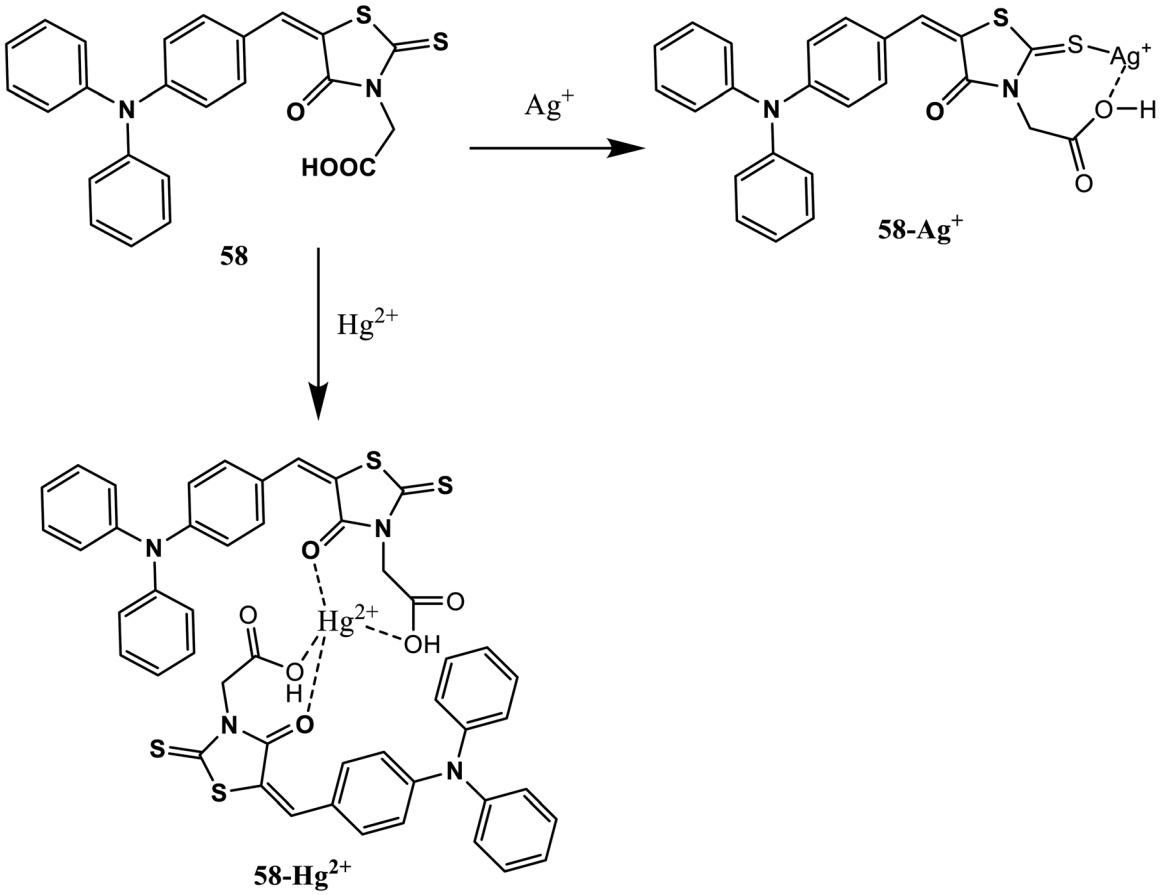

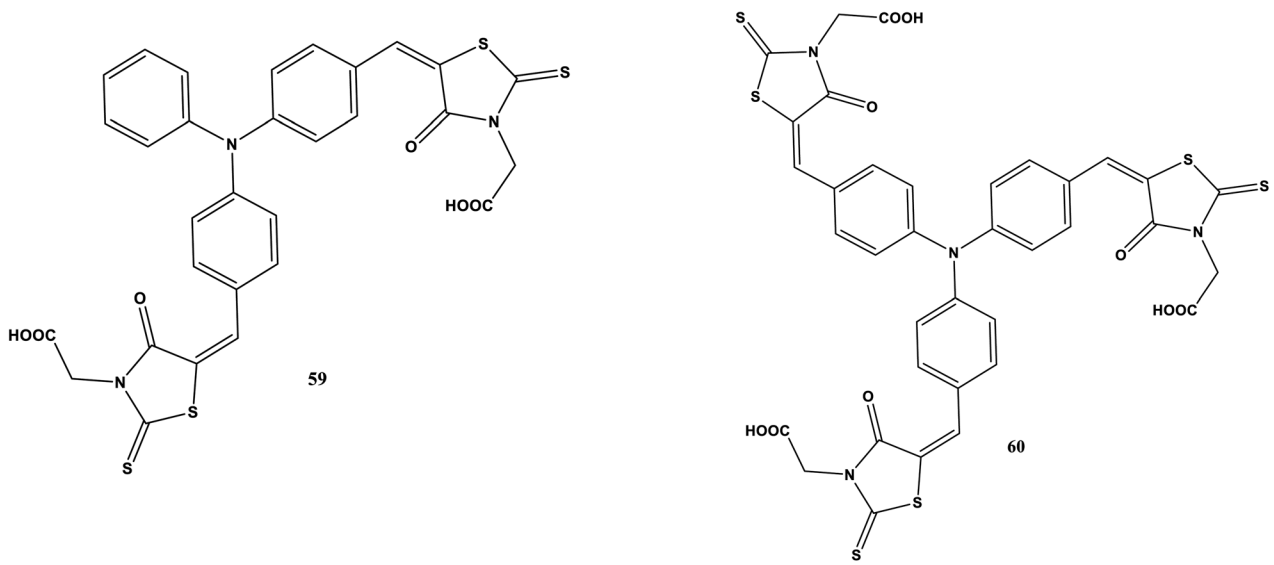

Fig. 15 (*contd.*)

Published on 14 February 2022. Downloaded by Bengal Engineering and Science University on 6/8/2022 1:03:11 PM.

significantly increased the fluorescence emission of the probe at 580 and 501 nm, respectively, with low detection limits.

Easwaramoorthi *et al.* designed and synthesized three probes **58–60** based on triphenylamine and rhodanine-3-acetic acid for the dual detection of Ag^+ and Hg^{2+} in buffer-free aqueous solutions.[92] All the three chemosensors showed distinct colour changes for Ag^+ and Hg^{2+} by the naked eye. Probe **58** in solution showed a change in color from yellow to purple or colorless in the presence of Ag^+ and Hg^{2+}, respectively. **59** and **60**, on the other hand, showed a colour change from pale brown to dark brown or purple in the presence of Ag^+ and Hg^{2+}, respectively. In the absorption spectrum, **58** exhibited red-shifted absorption from 476 to 486 nm in the presence of Ag^+ ions and blue-shifted absorption to 451 nm with Hg^{2+} ions. In the presence of Ag^+ ions, probe **58** showed fluorescence quenching with 88 nm red-shifted emission from 624 to 712. In the case of Hg^{2+}, however, it only exhibited a 12 nm red-shifted emission with fluorescence quenching. The authors proved that the difference in signalling for Ag^+ and Hg^{2+} is due to the different binding modes (Fig. 15). **59** and **60** also exhibited fluorescence quenching in the presence of both Ag^+ and Hg^{2+}, but the quenching behaviour was different because of the different numbers of rhodanine-3-acetic acid groups. The limit of detection was calculated for all three probes (**58**, **59** and **60**) and estimated as 7.59 μM, 5.12 μM, and 2.71 μM, respectively, for Ag^+, and 0.35 μM, 2.49 μM, and 1.96 μM, respectively, for Hg^{2+}. Moreover, cell imaging was also performed with HaCaT cells, and all three probes gave the same fluorescence quenching from red fluorescence in the presence of both ions.

4 Fluorescent probes based on a triphenylamine platform for neutral molecules

Triphenylamine derivatives for the detection of neutral molecules also have great importance. A neutral molecule means a molecule with no charge on it, such as diethylchlorophosphate (DCP), thiol, thiophenol, hydrogen sulfide, or hydrazine. These neutral molecules are also hazardous to all living things. So, it is necessary to detect these molecules by modulating a fluorescent probe.

4.1 Triphenylamine derivatives as fluorescent probes for diethylchlorophosphate

Organophosphorous compounds used as chemical warfare agents (CWA), also called nerve agents (NA), are hazardous to public health. However, diethylchlorophosphate (DCP) is affirmed as a nerve-agent mimic ascribable to its low toxicity but comparable reactivity to NAs, and so, cheap and easy detection of DCP is most desirable.

Yao *et al.* developed charge-transfer colorimetric and fluorescent probe **61** (Fig. 16a) for on-site monitoring of DCP vapor.[93] Probe **61** in THF exhibited two new absorption peaks at 294 and 410 nm, and the peak at 345 nm decreased upon the addition of DCP and the emission red-shifted from 412 nm to 472 nm. The authors rationalized the sensing mechanism by

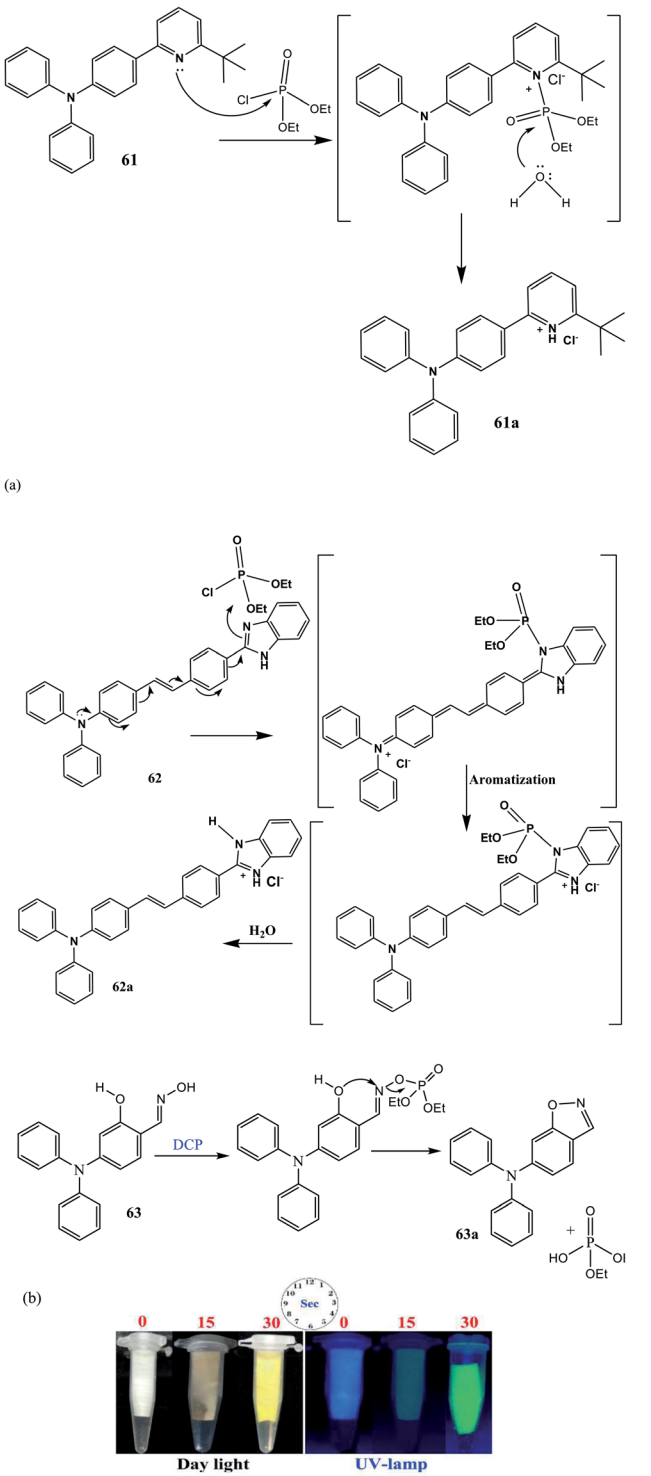

Fig. 16 (a) Structures of probes **61–63** and their probable sensing mechanisms with DCP. (b) Photographs of color and fluorescence responses of **63** upon exposure to DCP (0–10 equiv.) for 0–30 s. Photographs were taken in daylight and under a UV lamp. Reprinted from ref. 95. Copyright (2020), with permission from Elsevier.

NMR experiments and showed that the conversion of the pyridine group into pyridinium salt results in a dramatic red-shifted fluorescence for naked-eye detection of DCP.

This journal is © The Royal Society of Chemistry 2022

Published on 14 February 2022. Downloaded by Bengal Engineering and Science University on 6/8/2022 1:03:11 PM.

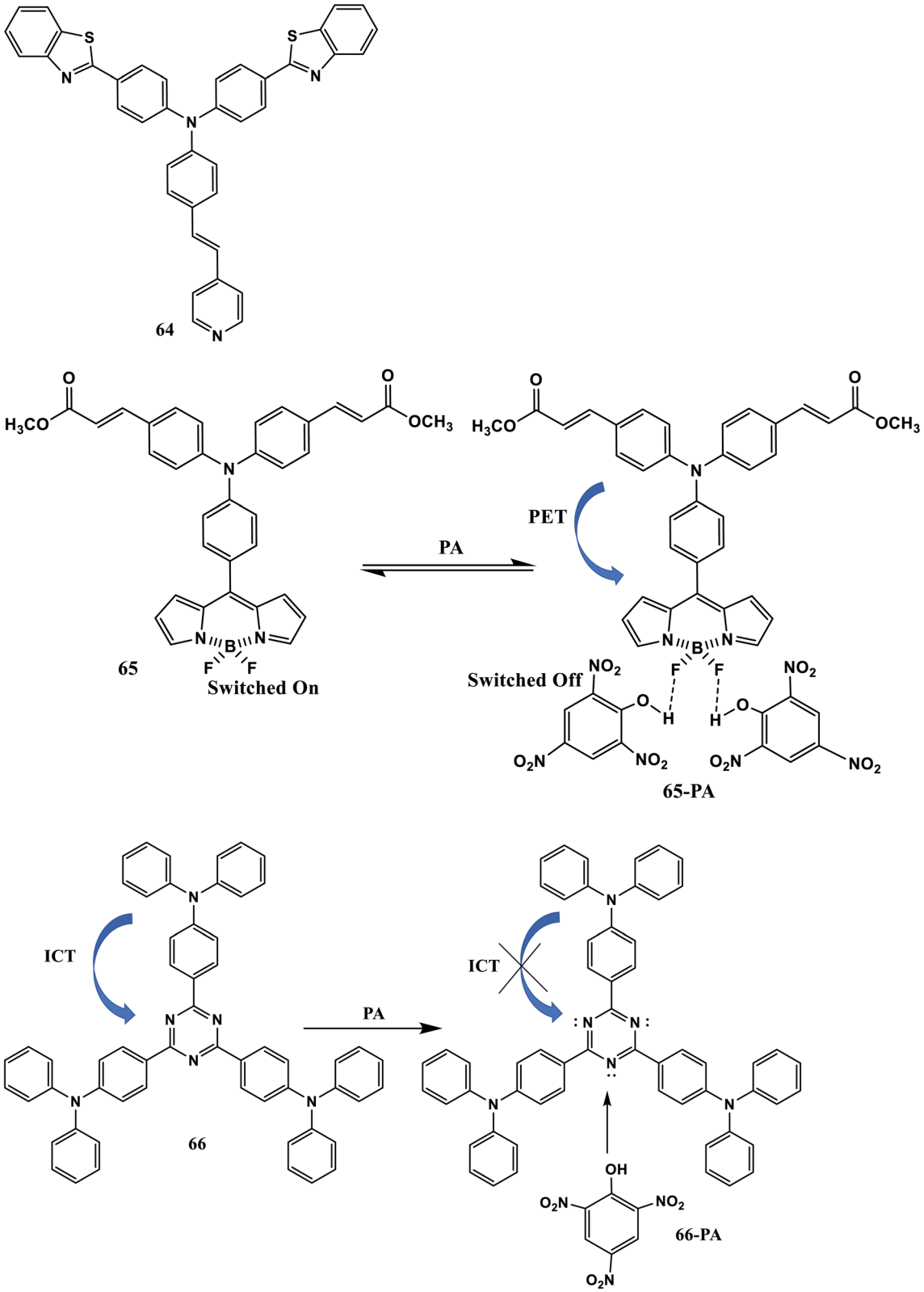

Fig. 17 Structures of probes 64–74 and probable sensing mechanisms of probes 65 and 66 with PA.

Published on 14 February 2022. Downloaded by Bengal Engineering and Science University on 6/8/2022 1:03:11 PM.

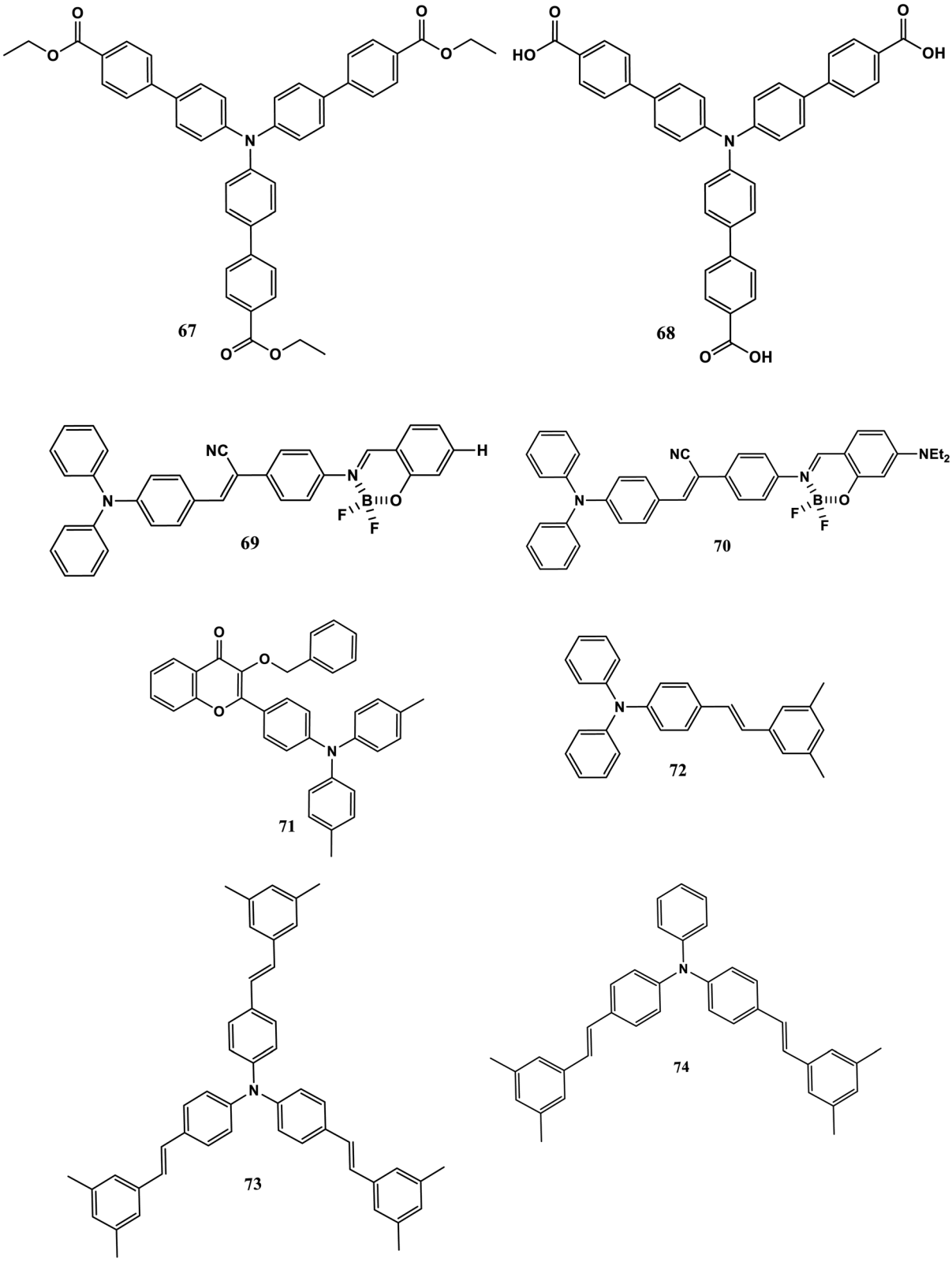

Fig. 17 (*contd.*)

 This journal is © The Royal Society of Chemistry 2022

Published on 14 February 2022. Downloaded by Bengal Engineering and Science University on 6/8/2022 1:03:11 PM.

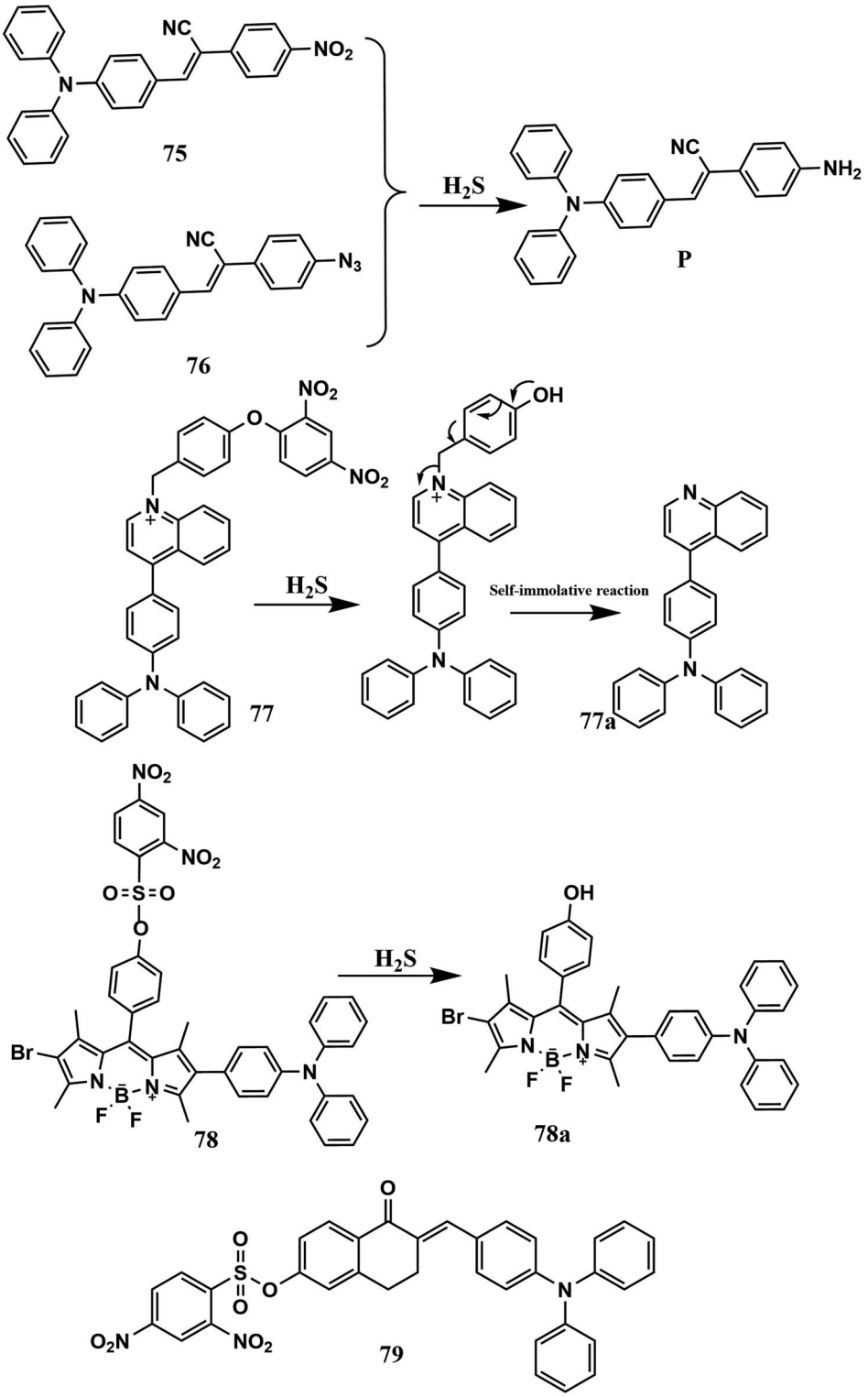

Fig. 18 Structures of probes 75–79 and probable sensing mechanisms of probes 75–78 with H_2S.

Mondal's group developed **62** (Fig. 16a) for the detection of DCP both in solution and in gaseous phase.[94] Most solution-phase DCP sensors have a pyridine group, an aliphatic or an aromatic hydroxyl group, an amine group, a carbonyl group, a spirobenzopyran group, an oxime group, or a carboxylic acid group, but probe **62** has a benzimidazole group, which acts as a receptor to sense DCP. Selectivity was measured by incorporating other mimicking agents such as diethyl cyanophosphonate (DECP), dimethyl methylphosphonate (DMMP), triethyl phosphate (TEP), or tributyl phosphate (TBP) into the THF/H_2O (4/1, v/v) solution, but only DCP showed a dramatic change in the spectra of the probe.

Published on 14 February 2022. Downloaded by Bengal Engineering and Science University on 6/8/2022 1:03:11 PM.

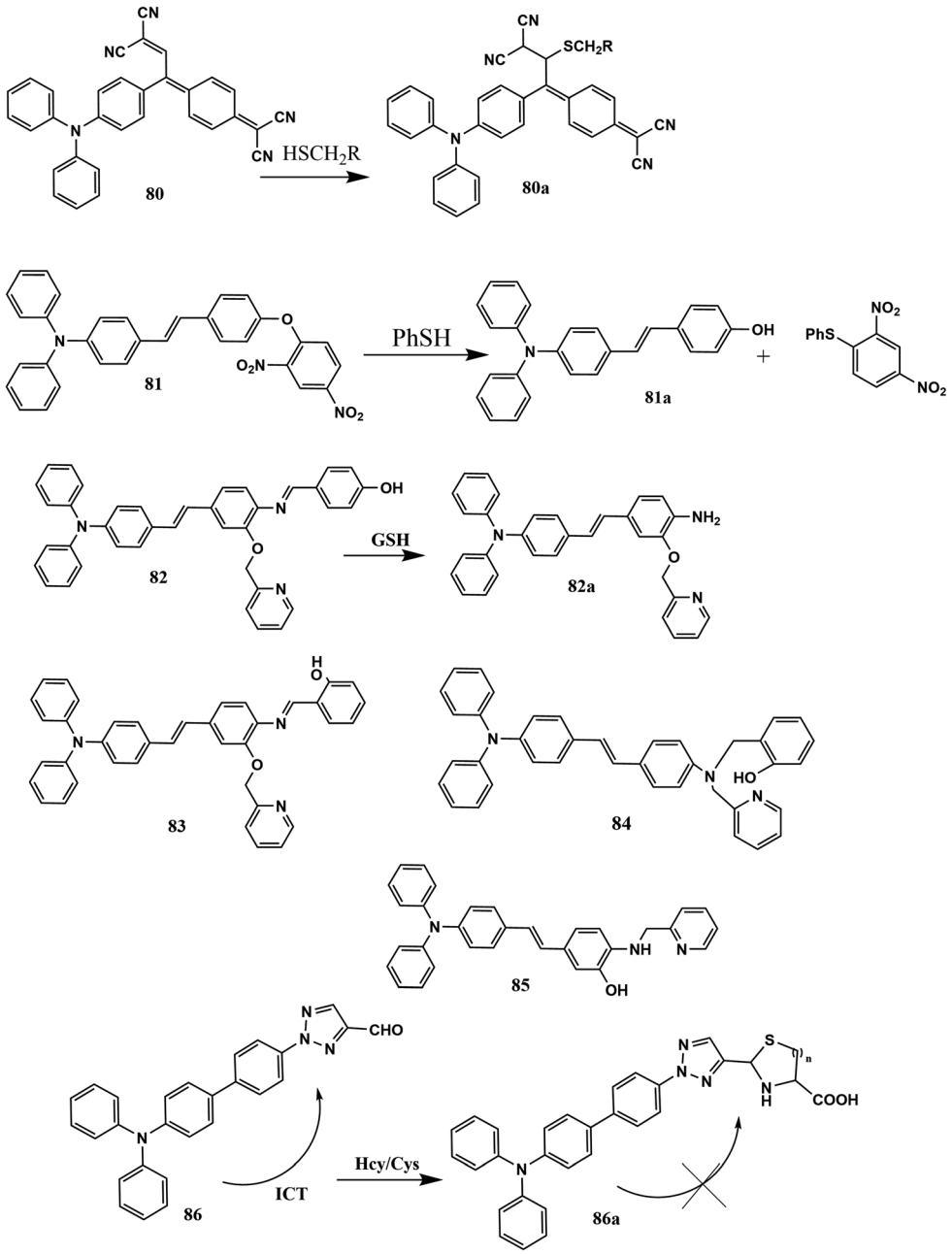

Fig. 19 Structures of probes 80–86 and probable sensing mechanisms of probes 80, 81, 82 and 86.

Mahapatra's group reported a new ratiometric probe **63** based on an *o*-hydroxyl-substituted triphenylaminoaldehyde oxime group that can recognise DCP in the vapour phase (Fig. 16a and b).[95] Probe **63** exhibits a ratiometric fluorescence change upon the addition of DCP. The authors proved that the stoichiometry of the formation of compound **63a** between probe **63** and DCP is 1 : 1. The detection limit of the probe was found to be 0.14 μM.

4.2 Triphenylamine derivatives as fluorescent probes for picric acid (PA)

Siva's group found that compound **64** (Fig. 17) in methanol : -water (80 : 20) exhibited an enhancement in absorbance at 400 nm with treatment by picric acid.[96] The enhancement in absorbance at 400 nm for PA can be ascribed to the formation of new species after the interaction between compound **64** and PA. Fluorescence intensity was strongly quenched at 500 nm with the addition of PA, whereas other aromatics exhibited only small changes. The quantum yield was decreased from 0.31 to 0.08 upon the addition of one equivalent of picric acid and the detection limit was found to be 23 ppm.

Hengchang *et al.* found that compound **65** (Fig. 17) was almost non-emissive in pure THF.[97] However, probe **65** could emit an intensified red color when 80% water was mixed. This observation confirms that the compound exhibits AIE

 This journal is © The Royal Society of Chemistry 2022

Published on 14 February 2022. Downloaded by Bengal Engineering and Science University on 6/8/2022 1:03:11 PM.

characteristics. The intermolecular photoinduced electron transfer (PET) could be enhanced in the presence of PA, as the BODIPY unit turns into a more electron-deficient centre, which results in fluorescence quenching at 650 nm. A practical application was presented in an artistic manner by cutting filter paper in a Tibetan language word to detect PA in a paper test strip.

Sathiyan *et al.* reported a star-shaped TPA-based probe **66** (Fig. 17) for the detection of ultratrace amounts of picric acid.[98] The absorbance peak of **66** increased at 394 nm upon the addition of PA. But the addition of other NACs (nitroaromatic compounds) to **66** did not cause any significant change in the absorption intensity. In a fluorescence study, it was found that the intense emission peak at 504 nm of the probe was quenched on the addition of PA.

Ziqiang's group reported two compounds **67** and **68** (Fig. 17) for the detection of picric acid in the solution phase as well as in the vapour phase.[99] For both probes, the fluorescence emission intensity rapidly decreased upon the addition of increasing amounts of PA solution, but, interestingly, the quenching efficiencies of **67** and **68** toward PA were found to be 82% and 95%, respectively. From scanning electron microscopy (SEM) images, the authors found that the interactions of **67** and **68** with PA, possibly through multiple hydrogen bonds, lead to breakdown in the assembly morphology of **67** and **68**.

Guo *et al.* developed two fluorescent probes, **69** and **70** (Fig. 17).[100] They exhibit a solvatochromic effect. For probe **69**, a hypsochromic-shift from 541 nm in benzene to 530 nm in ethanol was observed in the emission spectra. However, for probe **70**, a bathochromic shift was found from 516 nm in benzene to 540 nm in DMF. A solid-state emission study revealed that probe **69** exhibits orange fluorescence in the solid state, but probe **70** exhibits a bathochromic shift in the fluorescence peak, emitting yellow fluorescence due to an additional electron-donating group. The solid-state fluorescent quantum yields of **69** and **70** were measured as 13.5% and 19.4%, respectively, in the solid state. The fluorescence of both probes was quenched upon the addition of PA through the PET process.

Wang's group designed and reported a novel D–A-type flavonoid sensor **71** (Fig. 17) with AIEE properties, by incorporating a triphenylamine moiety as the electronic donor.[101] The free probe showed intense fluorescence at 525 nm in water, but after the addition of PA (from 0.5 to 25 equiv.), the intensity of fluorescence gradually decreased. The quenching degree of the compound towards 25 equiv. of PA could reach 96%. This quenching of emission can be attributed to the PET (photoinduced electron transfer) process and was supported by a DFT study.

Siva's group developed compounds **72–74** (Fig. 17) for the fluorometric detection of picric acid.[102] All these compounds have AIEE characteristics and give blue fluorescence in aqueous media. With an increasing number of styryl units from **72** to **74**, the electron-donating ability increases, which results in a bathochromic shift in absorption. The emission spectra of **72**, **73** and **74** are very sensitive to solvent polarity and a red-shift was observed with an increase in solvent polarity. When these three compounds were titrated with picric acid, a colour change from blue to pale yellow upon the addition of PA was observed due to charge transfer complex formation, and in the emission spectra, a decrease in emission was observed upon the addition of PA.

4.3 Triphenylamine derivatives as fluorescent probes for H_2S

Azido and nitro groups can be reduced to amine (NH_2) by H_2S. Depending on this mechanism Zhao *et al.* developed two AIE-based fluorescent probes **75** and **76** (Fig. 18) for the recognition of H_2S.[103] Probe **75** with the conversion of a nitro group to amine (P) upon the addition of H_2S showed a 91 nm blue-shifted emission band and the fluorescence intensity ratio (F_{616}/F_{525}) increased from 10.6 ± 0.1 to 0.72 ± 0.05. In the case of probe **76**, bearing an azido group, upon the addition of H_2S an 8-fold fluorescence increase at 570 nm was observed.

Dinitrophenyl acts as a good leaving group and is used in the fluorescent change mechanism. Depending on this, Xu *et al.* reported a triphenylamine-based AIE probe **77** (Fig. 18) for the detection of H_2S in food and also in biological systems.[104] Free probe **77** showed absorption at 500 nm and almost no fluorescence at 468 nm. The absorption was maximised at 400 nm and emission was enhanced at 468 nm upon the addition of H_2S. Detecting H_2S released in raw meats was the great application of probe **77**.

Based on the same fluorescence mechanism Quan *et al.* developed a triphenylamine–BODIPY-based NIR fluorescent probe **78** (Fig. 18) for the detection of H_2S in colorectal cancer cells.[105] Probe **78** shows two absorption bands at 450 nm and 527 nm, and both increase upon the addition of H_2S. The probe showed no fluorescence, but upon the addition of H_2S, beautiful fluorescence emission at 716 nm was noted. A biological application was studied with HCT116 cells and the detection limit was found to be 6.74 nM.

Recently, Hu's group developed **79** (Fig. 18) for the recognition of H_2S based on the mechanism of the DNP group leaving.[106] The probe showed a maximum absorption peak at 420 nm. The fluorescence intensity at 550 nm ($\lambda_{ex} = 420$ nm) increased from a very weak level as the concentration of sodium sulfide increased. The fluorescence quantum yield (Φ_F) of **79** increased from 0.02 to 0.23 upon treatment with sodium hydrosulfide.

4.4 Triphenylamine derivatives as fluorescent probes for thiol/thiophenol

Tang *et al.* designed and synthesized probe **80** (Fig. 19) to detect thiols.[107] Probe **80** in MeCN shows a colorimetric response with a visible color change from yellow green to colorless upon the addition of thiols. Probe **80** shows two absorption bands with one intense ICT band at 426 nm and the other a lower-energy ICT band at 710 nm. Upon the addition of cysteine (Cys), these two bands decreased, and a new band appeared at 300 nm, indicating inhibited ICT. Other thiols, such as Hcy and GSH, gave quite similar but smaller variations, but other amino acids gave no significant response.

Published on 14 February 2022. Downloaded by Bengal Engineering and Science University on 6/8/2022 1:03:11 PM.

Wang *et al.* reported a novel triphenylamine-based probe **81** (Fig. 19) for the selective detection of thiophenols.[108] Probe **81** exhibited a clear enhancement in the fluorescence response with the addition of thiophenol in a solution of DMSO/PBS (5/5, v/v). Because of the strong electron-withdrawing property of the 2,4-dinitrophenyl core, probe **81** showed almost no emission in fluorescence, but after the addition of thiophenol, it displayed a 200-fold fluorescence enhancement at 435 nm as the 2,4-dinitrophenyl moiety quickly reacted with thiophenol and left the triphenylamine moiety, with a clear color change from almost colorless to bright blue-green under a 365 nm UV lamp.

A series of probes **82–85** (Fig. 19) based on triphenylamine with a C=N– or NH– group, were designed and synthesized by Yang's group.[109] Probes **82–85** can recognise GSH by two mechanistic pathways, where **82** and **83** can directly detect it by hydrolysis, but detection by **84** and **85** occurs *via* complex formation with Cu^{2+} and a demetallation effect. However, all four were applied for detection in living (HeLa) cells.

Most biothiol sensors mainly used to detect Hcy/Cys, cannot selectively detect either Hcy or Cys. So, designing a sensor that can selectively detect one of them is a challenging task. Finally, Chu *et al.* designed a novel probe **86** (Fig. 19), which can recognise Hcy with high selectivity.[110] However, probe **86** could not distinguish Hcy/Cys in absorption spectra, but in fluorescence spectra, the compound exhibited a remarkable change in fluorescence at 459 nm in the presence of Hcy, but in the presence of Cys there was negligible enhancement in fluorescence.

4.5 Fluorescent probes for hydrazine

Niamnont's group created triphenylamine-based fluorophore **87** (Fig. 20) for identifying hydrazine in the vapour phase.[111] A combination of cellulose acetate (CA) with an electrospun nanofiber sheet formed probe **87** using an electrospinning technique where the average diameter was 324.6 ± 91.6 nm. The sensing nanofiber sheet showed a sensitive and selective reaction to hydrazine vapor with a linear concentration range of 0.2–1 w/v% in aqueous solution.

Recently, Mahapatra *et al.* designed and synthesized **88** (Fig. 20) for the detection of hydrazine in real water samples and also in living cells.[112] The probe shows solvatochromism. By changing the solvent from CCl_4 to DMSO, a 102 nm red-shifted emission was observed. In the case of hydrazine sensing, the absorption band of **88** in DMSO changed with the addition of hydrazine. For emission spectra, various solvent systems (CCl_4, MeOH, DMSO) were used. In the case of CCl_4, there was no change in emission spectra, but in the case of MeOH and DMSO, spectral changes were observed upon the addition of hydrazine.

Ding *et al.* reported two bis-Schiff bases **89** and **90** (Fig. 20) to recognize hydrazine.[113] Probes **89** and **90** in an aqueous solution of DMF exhibited fluorescence quenching at 560 nm upon the addition of hydrazine. Both had the same low detection limit of 55.1 nM. The authors also showed a biological application of the probe for the detection of hydrazine in living cells.

Wang *et al.* recently designed and synthesized triphenylamine-based fluorescent dye **91** (Fig. 20) for the rapid detection of hydrazine *in vivo* and *in vitro*.[114] With the addition of hydrazine, the phenyl ester bond of **91** was reduced to –OH and formed **91a** due to the strong reduction property of hydrazine, resulting in an obvious 'naked eye' colour change from cyan to bright blue under a 365 nm UV lamp. The molecule showed increased emission in the solid state rather than in the

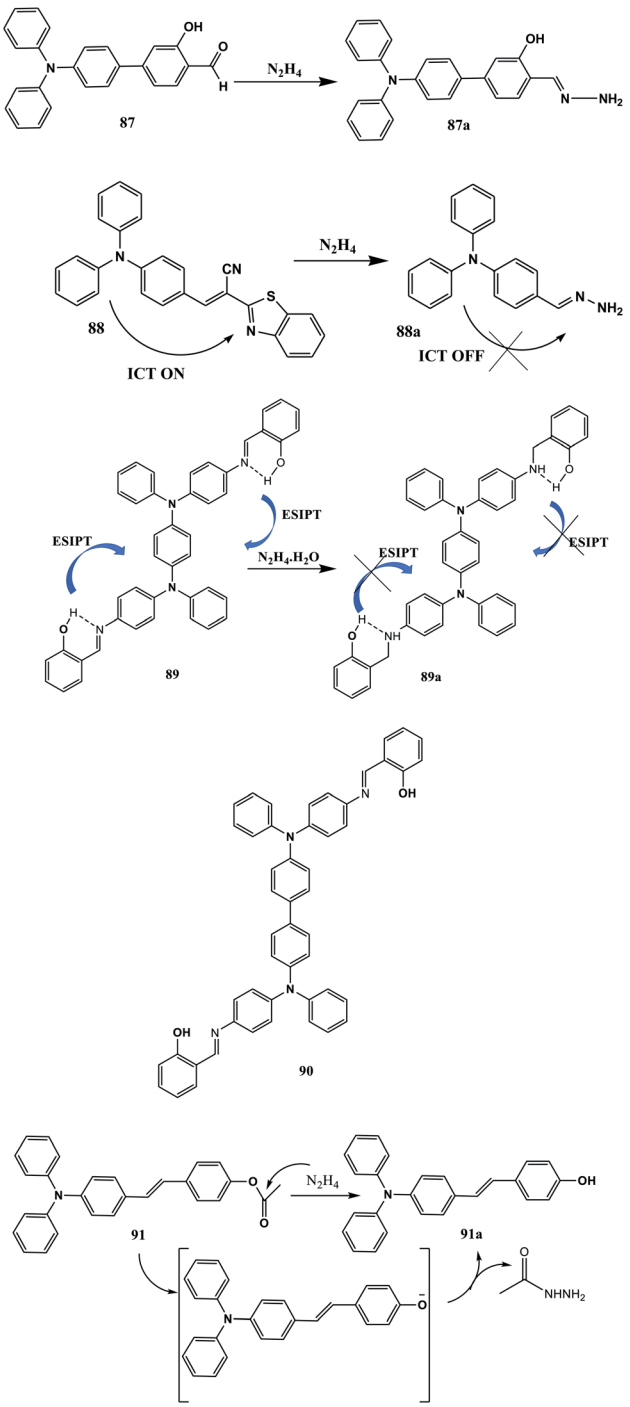

Fig. 20 Structures of probes **87–91** and probable sensing mechanism of probes **87**, **88**, **89** and **91** with N_2H_4.

 This journal is © The Royal Society of Chemistry 2022

Published on 14 February 2022. Downloaded by Bengal Engineering and Science University on 6/8/2022 1:03:11 PM.

Table 1 Summary of significant photophysical properties and applications of various fluorescent probes

Probe for analyte	Probe type/ sensing mech	Media	Excitation	Emission	Quantum yield (Φ) in absence/ presence of analyte	Binding/ stability/ association/ quenching constant	LOD	Application	Ref.
1 for CN^-	Turn-on/ICT	EtOH–Tris·HCl buffer solution (10.0 mM, PH = 7.4, 4 : 6, v/v)	345 nm	445 nm	—	—	21 nM	Detection in living cells (GES cells)	28
2 for CN^-	Turn-on/ICT	EtOH : H_2O (1 : 1, v/v, HEPES buffer, pH 9.3)	365 nm	477 nm	—	—	50 nM	Detection in living cells (HepG2 cells)	29
3 for CN^-	Turn-off	CH_3CN/H_2O (9/1, v/v)	650 nm	780 nm	—	—	14 nM in CH_3CN and 0.23 μM in CH_3CN/H_2O (9/1, v/v)	Detection in living cells (L929 cells)	30
4 for CN^-	Turn-on	ACN–H_2O (1 : 9 v/v, PBS buffer, pH 7.2)	450 nm	565 nm	—	—	4.24×10^{-8} M	Detection in living cells	31
5 for CN^-	Turn-on/AIE	DMF/PBS (1 : 99, v/v)	—	596 nm	0.124 to 0.314	—	0.35 μmol L^{-1}	Detection in living cells (HepG2 cells)	32
6 for CN^-	Turn-on/ICT	CH_3CN/100 mM HEPES buffer pH 10.0 (9 : 1 v/v)	368 nm	460 nm	Below 0.05	—	0.68 μM	Detection in real water samples	33
7 for CN^-	Turn-on	DMF : HEPES buffer (4 : 6)	320 nm	400 nm	—	—	44 nM	Detection in test strips	34
8 for CN^-	Turn-on	THF/H_2O (99 : 1, v/v)	480 nm	627 nm	0.23	—	0.014 μM		35
9 for CN^-	Turn-off/ICT	THF	510 nm	606 nm↓	—	—	0.46 nM		36
10, **11** for CN^-	Turn-off (**10**) Turn-on/ICT (**11**)	DMSO–H_2O	438 nm (**10**) 466 nm (**11**)	608 to 597 nm (**11**)	—	—	0.087 μM (**11**)	Detection in living cells (BEAS-2B) and in food samples (**11**)	37
12 for CN^-	Turn-on/ICT	THF/water (v/v = 9/1)	430 nm	551 nm	—	—	14 nM	Detection in (a) real water samples and (b) living cells (PC12)	38
13 for CN^-	Turn-on	MeCN/H_2O (v/v, 9/1)		430 and 445 nm	0.522	5.36	0.23 μM	Detection in real water samples	39
14, **15** for CN^-	Turn-on/ICT	DMSO		614 nm to 574 nm (**14**)	—	2.7×10^2 M^{-1} (**14**)	234 nM (**14**)	Detection in living cells (HeLa cells)	40
				604 nm to 564 nm (**15**)		10×10^2 M^{-1} (**15**)	11 nM (**15**)	Detection in molecular electronics and nanodevices	
16 for CN^-	Turn-on/ICT	DMSO	365 nm	581 nm	—	—	2.95×10^{-8} mol L^{-1}		41

Published on 14 February 2022. Downloaded by Bengal Engineering and Science University on 6/8/2022 1:03:11 PM.

Table 1 (*Contd.*)

Probe for analyte	Probe type/ sensing mech	Media	Excitation	Emission	Quantum yield (Φ) in absence/ presence of analyte	Binding/ stability/ association/ quenching constant	LOD	Application	Ref.
								Detection in test strips	
17 for CN^-	Turn-on/ICT	CH_3CN/H_2O	272	402	—	—	0.36 μM	Detection in test strips	42
18, **19** for F^-	Turn-off/PET	CH_3CN/0.1% DMSO	330 nm (**18**)	462 nm (**18**)	—	$1.52 \pm 0.13 \times 10^4\ M^{-1}$ (**18**)			43
20 for F^-	Turn-on/ICT	(i) Acetone (ii) Acetonitrile		(i) 590 nm to 641 nm (ii) 631 nm	—	—	(i) 4.20 μM (ii) 2.46 μM	Acts as logic function in acetonitrile	44
21 for F^-	Turn-on/PET	THF–H_2O (1 : 9 v/v)	367 nm	450 nm	—	—	2.74×10^{-8} M	Detection in living cells (HEK-293 cells)	45
22 for F^-	Turn-on (THF), ratiometric turn-off (ACT), ratiometric turn-on (ACN)	THF, ACT, ACN	443 nm	575 nm (THF) 579 nm↓487 nm↑(ACT) 484 nm↑547 nm↓(ACN)	2.9% (amorphous) 4.9% (crystal)	—	0.0064 vol% (THF), 0.0042 vol% (ACT), 0.192 vol% (ACN)	Detection of water content of commercial products	46
23 for F^-	Turn-off/ICT	DCM		430 nm	—	11 : 00 ± 0 : 08			47
24 for OCl^-	Turn-on/ ratiometric	THF/H_2O, 2 : 3, v/v	430 nm	630 nm↓, 485 nm↑	0.28		7×10^{-8} M	Detection in living cells	50
25 for OCl^-	Turn-off	DMSO/PBS buffer solution (1 : 4, v/v, 10 mM) PBS buffer, pH 7.4)	375 nm	523 nm	—	—	0.8 μM	Detection in living cells (A549 cells)	51
26 for OCl^-	Turn-on	THF/PBS buffer solution (1 : 1, v/v, PBS buffer, pH 7.4)	450 nm	520 nm	0.02 to 0.43	—	7.37×10^{-7} M	Detection in real water samples	52
27 for OCl^-	Turn-on/TICT, AIE	10 mM PBS buffer pH 7.4	365 nm	514 nm	0.157	—	13.2 nM	Detection in living cells (HeLa cells)	53
28 for OCl^-	Turn-on/ICT	DMSO/H_2O (v/v, 5 : 1)	408 nm	605 nm	—	—	64.2 nM	Detection in living cells (MRC-5 cells)	54
29 for $ONOO^-$	Turn-on/ ratiometric	PBS buffer (pH = 7.4)		650 nm, 485 nm	—	—	12.1 nM	Detection in living cells (HepG2)	55
30 for Cu^{2+}	Turn-on	(i) CH_3CN	(i) 380 nm	(i) 472 nm	0.374	(i) $1.96 \times 10^7\ M^{-1}$	(i) 1.8×10^{-7} M	Detection in real water samples	68
		(ii) CH_3CN/H_2O (v/v = 4/6, pH = 7.4)	(ii) 360 nm	(ii) 506 nm		(ii) $5.43 \times 10^7\ M^{-1}$	(ii) 8.5×10^{-7} M		
31 for Cu^{2+}	Turn-off	CH_3CN/H_2O (70/30, v/v)	291 nm	378 nm		$(3.59 \pm 0.29) \times 10^5$	20 μM		69

This journal is © The Royal Society of Chemistry 2022

Published on 14 February 2022. Downloaded by Bengal Engineering and Science University on 6/8/2022 1:03:11 PM.

Table 1 (*Contd.*)

Probe for analyte	Probe type/ sensing mech	Media	Excitation	Emission	Quantum yield (Φ) in absence/ presence of analyte	Binding/ stability/ association/ quenching constant	LOD	Application	Ref.
32 for Cu^{2+}	Turn-off	DMSO/H_2O (1 : 1, v/v)	370 nm	476 nm	0.321 to 0.008	—		Detection in living cells (HepG2, A549 and HeLa cells)	70
33 for Cu^{2+}	Turn-on	CH_3CN		637 nm	—	1.184×10^4 M^{-1}	1.568×10^{-6} M		71
34 for Cu^{2+}	Turn-off	CH_3CN	340	408	—	6.57×10^4 M^{-1}	3.93×10^{-6} mol L^{-1}		72
35, **36** for Al^{3+}	Turn-on/CHEF	CH_3OH–H_2O (v/v, 4 : 1)		450 nm to 489 nm (**35**)	< 1% (**35**)	6.65×10^3 M^{-1} (**35**)	1.22×10^{-7} M (**35**)	Detection in living cells	73
					<1% to 9.21% (**36**)	7.70×10^4 M^{-1} (**36**)	2.99×10^{-7} M (**36**)		
37 for Al^{3+}	Turn-on/AIE	DMSO/HEPES mixture (v/v, 1 : 1, pH = 7.0)	450 nm	580 nm	—	—	1.5×10^{-7} M	Detection in living cells (HeLa cells)	74
38 for Fe^{3+}	Turn-off/AIE, PET	THF	300 nm	470 nm	—	—	4.51×10^{-5} M	Detection in living cells (PC-3 cells)	75
39 for Fe^{3+}	Turn-off/ICT	DMSO		445 nm	—	—	0.511 μM	Detection in living cells (HeLa cells)	76
40 for Fe^{3+}	Turn-off	THF		523	0.326	3.5×10^3 M^{-1}	1.01×10^{-7} M	Detection in living cells (HeLa cells)	77
41 for Hg^{2+}	Turn-on/PET	DMSO/Tris–HCl (8/2, v/v)	375 nm	487 nm	0.173	7.485×10^7 M^{-1}	3.11×10^{-8} M	Detection in test strips	78
42 for Hg^{2+}	Turn-on/ ratiometric	THF/H_2O (99 : 1, v/v)	587 nm	656 nm↓, 723 nm↑	0.0665	—	0.36 μM	—	79
43 for Hg^{2+}	Turn-on/ ratiometric	THF/H_2O (99 : 1, v/v)	485 nm	600 nm↓, 650 nm↑	13.3%	—	0.089×10^{-6} M	—	80
44 for Hg^2	Turn-off	DMF	277	462	—	—	1.23×10^{-7} M	Detection in test strips	81
45 for Cr^{3+}	Turn-on	THF	320	431	28%	2.8×10^4 M^{-1}	1.5×10^{-6} M	—	82
46 for Sn^{2+}	Turn-on/ICT, CHEF	H_2O–DMSO (1 : 1, v/v)	320	460	24%	6.8×10^9 M^{-2}	3.14×10^{-7} M	—	83
47 for Zn^{2+}, Cd^{2+}	Turn-on	CH_3CN	400 nm	595 nm (Cd^{2+}) 620 nm (Zn^{2+})	—	$(1.08 \pm 0.13) \times 10^5$ M^{-1} for Cd^{2+} and $(1.30 \pm 0.18) \times 10^5$ M^{-1} for Zn^{2+}	$(3.43 \pm 0.21) \times 10^{-6}$ M for Cd^{2+} and $(3.16 \pm 0.18) \times 10^{-6}$ M for Zn^{2+}	—	84

Published on 14 February 2022. Downloaded by Bengal Engineering and Science University on 6/8/2022 1:03:11 PM.

Table 1 (*Contd.*)

Probe for analyte	Probe type/ sensing mech	Media	Excitation	Emission	Quantum yield (Φ) in absence/ presence of analyte	Binding/ stability/ association/ quenching constant	LOD	Application	Ref.
48, **49** for Zn^{2+}, Cd^{2+}	Turn-on	CH_3CN	360 nm	488 nm (Zn^{2+}) 458 nm (Cd^{2+}) (1st fluorescence) 488 to 466 nm (Cd^{2+}) (2nd fluorescence) (**48**) 458 to 466 nm (Zn^{2+}) (2nd fluorescence (**48**) 488 to 466 nm (Cd^{2+}) (2nd fluorescence) (**49**) 458 to 466 nm (Zn^{2+}) (2nd fluorescence) (**49**)	—	—	—	—	85
50, **51** for Hg^{2+}, Fe^{3+}	Turn-off/PET	CH_3CN	350 nm (**50**)	438 nm (**50**)	1.3%	—	—	—	86
52 for Hg^{2+}, Cu^{2+}	Turn-on (Cu^{2+})	MeCN/H_2O (9/1)	350 nm	441 and 458 nm	0.061 for Hg^{2+}	6.02 M^{-1} for Hg^{2+}	2.39 μM for Hg^{2+}	—	87
53 for Fe^{3+}, Cu^{2+}	Turn-on/ ratiometric	CH_3CN	—	425 nm↓, 362 nm↑ for Fe^{3+}	0.6% for Fe^{3+}	—	230 nM for Fe^{3+}	—	88
				425 nm↓, 362 nm↑ for Cu^{2+}	1.5% for Cu^{2+}		620 nM for Cu^{2+}		
54, **55** for Fe^{3+}, Al^{3+}	Turn-on (**55**)	CH_3CN (**54**) DMF (**55**)	365 nm (**55**)	513 nm (**55**)	—	2.645×10^6 mol^{-1} (**55**)	6.0 μM (**55**)	—	89
56 for Zn^{2+}, CN^-	Turn-on (Zn^{2+})	(DMF : buffer = 1/2, v/v pH = 7.24)	350 nm	565 nm↑ for Zn^{2+}	—	1.68×10^{19} M^{-2} for Zn^{2+}	14 nm for Zn^{2+}	Detection in living cells (MCF-7 cells)	90
	Turn-off (CN^-)			565 nm↓ for CN^-		1.7×10^3 for CN^-	0.37 μM for CN^-		
57 for Hg^{2+}, Al^{3+}	Turn-on/PET (Al^{3+}), FRET (Hg^{2+})	MeCN/H_2O (v/v, 9/1)	365 nm	501 nm for Al^{3+} 580 nm for Hg^{2+}	—	—	71.8 nM for Al^{3+} 0.48 μM for Hg^{2+}	—	91
58, **59**, **60** for Ag^+, Hg^{2+}	Turn-off (Ag^+)	THF/H_2O	—	~625 (**58**, **59**, **60**)	0.46 (**58**)	8.2×10^5 (**58**), 3.32×10^6 (**59**), and 1.05×10^5 M^{-1} (**60**) for Ag^+	7.59 (**58**), 5.12 (**59**), and 2.71 μM (**60**) for Ag^+	Detection in living cells (HaCaT cells)	92
	Turn-off (Hg^{2+})					2.4×10^5 (**58**), 4.6×10^5 (**59**), and 2.5×10^5 M^{-1} (**60**) for Hg^{2+}	0.35 (**58**), 2.49 (**59**), 1.96 μM (**60**) for Hg^{2+}		
61 for DCP	Turn-on/ ratiometric	THF		412 nm↓, 472 nm↑	~93%	—	2.6 ppb	—	93
62 for DCP	Turn-on/ ratiometric	THF/H_2O (4 : 1, v/v)	390 nm	483 nm, 573 nm	—	—	8.45×10^{-8} M	—	94
63 for DCP	Turn-on/ ratiometric	CH_3CN–H_2O (4 : 6, v/v)	379 nm	463 nm, 532 nm	—	—	0.14 μM	(i) Detection in living cells (Vero 76 cells) (ii) Detection in soil sample	95

This journal is © The Royal Society of Chemistry 2022

Published on 14 February 2022. Downloaded by Bengal Engineering and Science University on 6/8/2022 1:03:11 PM.

Table 1 (*Contd.*)

Probe for analyte	Probe type/ sensing mech	Media	Excitation	Emission	Quantum yield (Φ) in absence/ presence of analyte	Binding/ stability/ association/ quenching constant	LOD	Application	Ref.
64 for PA	Turn-off/ICT	CH_3OH–H_2O (80 : 20)	—	500 nm	0.31	—	23 ppm	—	96
65 for PA	Turn-off/PET	THF/hexane	500 nm	650 nm	—	2.1×10^{-6} M^{-1}	3×10^{-8} M	—	97
66 for PA	Turn-off/ICT	THF	396 nm	504 nm	—	3.5×10^{5} M^{-1}	0.37 nM	Detection in test strips	98
67, **68** for PA	Turn-off	THF	—	455 nm (**67**)	6% (**67**)	2.98×10^{-6} M^{-1} (**67**)	50 ppb (**67**)	(i) Detection in vapour phase	99
				450 nm (**68**)	18% (**68**)	14.3×10^{-6} M^{-1} (**68**)	4 ppb (**68**)	(ii) Detection in test strips	
69, **70** for PA	Turn-off/PET	THF/water (2 : 8, v/v)	—	—	13.5% (**69**) 19.4% (**70**)	—	1.26×10^{-6} M (**69**) 1.51×10^{-6} M (**70**)	—	100
71 for PA	Turn-off/AIEE	DMSO	395 nm	525 nm		1.93×10^{4} M^{-1}	370 nM	—	101
72–74 for PA	Turn-off	THF/H_2O (5 : 5)	362 nm (**72**)	430 nm (**72**)	—	—	30 ppb (**72** & **73**), 40 ppb (**74**)	Detection in test strips	102
75, **76** for H_2S	Turn-on/ ratiometric	DMF/PBS buffer (v/v, 4 : 6, pH 7.4)	—	616 nm↓, 525 nm↑ (**75**) 570 nm (**76**)	—	—	6.87 μM (**75**) 0.52 μM (**76**)	Detection in living cells (HeLa cells)	103
77 for H_2S	Turn-on	pH 7.4 PBS, 10 mM, containing 1% DMSO	—	468 nm	—	—	0.17 μM	(i) Detecting the released H_2S in raw meat samples (ii) Tracking the fluctuation of H_2S levels in living cells (iii) Imaging H_2S in tumor tissues	104
78 for H_2S	Turn-on	THF/PBS buffer (v/v = 4 : 1, pH = 7.4)	527 nm	716 nm	—	—	6.74 nM	Detection in living cells (HCT116 cells)	105
79 for H_2S	Turn-on/PET	THF–PBS solvent (30% THF, v/v, pH 7.4)	420 nm	550 nm	0.02 to 0.23	—	27.3 nmol L^{-1}	Detection in living cells	106
80 for thiol	Colorimetric	MeCN–HEPES buffer solution (1 : 1, v/v, HEPES, pH 7.4)	—	—	—	—	—	—	107
81 for thiophenol	Turn-on	(DMSO/PBS (5/5, v/v), pH = 7.4)	375 nm	435 nm	0.0046	—	4.5 nM	(i) Detection in real water samples (ii) Detection in living cells	108

Published on 14 February 2022. Downloaded by Bengal Engineering and Science University on 6/8/2022 1:03:11 PM.

Table 1 (*Contd.*)

Probe for analyte	Probe type/ sensing mech	Media	Excitation	Emission	Quantum yield (Φ) in absence/ presence of analyte	Binding/ stability/ association/ quenching constant	LOD	Application	Ref.
82–85 for GSH	Turn-on	DMSO : H_2O (4 : 1, v/v)	—	—	—	1.7343×10^5 M^{-1} (**82**) 6.0098×10^4 M^{-1} (**83**) 6.7063×10^5 M^{-1} (**84**) 6.4061×10^5 M^{-1} (**85**)	0.106 μM (**82**) 0.131 μM (**83**) 0.269 nM (**84**) 0.977 nM (**85**)	Detection in living cells (HeLa cells)	109
86 for Hcy, Cys	Turn-on ICT	CH_3CN/H_2O (v/v = 19 : 1, PBS, pH = 7.4)	362 nm	459 nm	7.22%	—	3.05×10^{-6} M	Detection in living cells (HeLa cells)	110
87 for hydrazine	Turn-on/ ratiometric	DMSO	370 nm	535 nm 455 nm	—	—	9 mM	(i) Detection in real water samples (ii) Detection in nanofibrous sheet	111
88 for hydrazine	Turn-on/ ratiometric	DMSO : H_2O, 3 : 7, v/v, HEPES buffer, pH 7.4	447 nm	611 nm↓, 514 nm↑	—	—	204 nM	(i) Detection in gas phase (ii) Detection in real water sample (iii) Detection in living cells (MC3T3 cells)	112
89, **90** for hydrazine	Turn-off/AIE, ESIPT	DMF/H_2O (50/50, v/v)	330 nm	560 nm	0.361 (**89**) 0.358 (**90**)		55.1 nM	Detection in living cells	113
91 for hydrazine	Turn-on	DMSO/PBS (4/6, v/v, pH = 7.40)	350 nm	440 nm	—	—	8.47 nM	Detection in living cells (HeLa cells)	114

This journal is © The Royal Society of Chemistry 2022

Published on 14 February 2022. Downloaded by Bengal Engineering and Science University on 6/8/2022 1:03:11 PM.

solution state. This observation is due to the restricted rotation of the probe in the solid state, and this was proved by the authors in a single-crystal X-ray study (Table 1).

5 Conclusion and perspective

In this review, we have shown how triphenylamine has been enormously used as a fluorescent probe targeting different analytes, varying from inorganic anions, to neutral analytes, to metal cations. Due to the notorious electron-donating ability of triphenylamine, researchers have been attracted to developing various fluorescent probes incorporating electron-withdrawing groups. Triphenylamine itself is nonfluorescent, but its simple functionalisation may generate a fluorescent property. In recent years, triphenylamine has appeared as a strong and amenable platform and we expect a shining future for triphenylamine derivatives in the field of fluorescence sensing. Based on a literature survey, triphenylamine-based fluorescent probes can be divided into three categories based on the type of analyte. These three are: (a) anion, (b) cation, and (c) neutral analyte fluorescent probes. They can be further divided by mode of mechanism. For selected cases (cyanide ions) of anion sensors, different sites of attack are present, such as (i) the indole moiety as the site of attack, (ii) cyanovinyl as the centre of attack, (iii) dicyanovinyl as the centre of attack, and (iv) other sites of attack. On the other hand, the fluoride ion sensing properties are observed mainly *via* hydrogen bond formation. Intriguingly, for hypochlorite ions, different types of chemodosimetric attack take place for signal or sensing. Again, for cations, we can observe that the signalling occurs chiefly *via* coordination of the probe with the metal ions. We also noticed some different signalling approaches for neutral analytes. Other than that, there are a variety of mechanisms involved in signalling for any analyte, namely, PET, ICT, ESIPT, CHEF, AIE, *etc.* Although most of the probes give fluorescence responses *via* ICT.

In spite of recent advances in the field, there are still some drawbacks. (i) In this literature, we find that many of the probes for detecting an analyte go through a 'turn-off' response, although 'turn-on' fluorescence has a greater impact on the selective and sensitive detection of analytes. So, it will be challenging to develop fluorescent probes which can detect analytes more powerfully by a 'turn-on' response. (ii) For *in vivo* applications in bioimaging, a triphenylamine scaffold should be allowed to emit in the NIR region, but in this review, there are very few probes whose emission was found in the NIR range. So, chemists should focus on designing a triphenylamine-based probe for NIR detection of an analyte. (iii) Moreover, in this review, we have discussed several mechanisms, such as PET, ICT, ESIPT, CHEF, and AIE, but other photophysical mechanisms, such as TBET (through-bond energy transfer), TSCT (through-space charge transfer), should also be looked into when designing a molecule. (iv) In this review, most probes are soluble in either organic solvent or organo-aqueous solvent. There are no probes which are soluble in pure water. However, the solubility of the probes plays a crucial role in biocompatibility. Poor water solubility of the probes should be considered a disadvantage and should be resolvable in the near future.

In the end, we hope that this review will help to develop more powerful fluorescent probes, which should be selective, sensitive, have good solubility in aqueous media, be biocompatible, and have a low detection limit and high quantum yield for useful and exciting applications.

Conflicts of interest

The authors declare no conflict of interest for this manuscript.

Acknowledgements

AK thanks IIEST, Shibpur for sponsoring the institute fellowship.

References

1 J. P. Menzel, H. J. M. de Groot and F. Buda, *J. Phys. Chem. Lett.*, 2019, **10**, 6504–6511.
2 H. B. Kim and J. J. Kim, *Org. Electron.*, 2018, **62**, 511–515.
3 Q. Hu, K. Ma, Y. Mei, M. He, J. Kong and X. Zhang, *Talanta*, 2017, **167**, 253–259.
4 C. A. Guido, B. Mennucci, D. Jacqueminc and C. Adamo, *Phys. Chem. Chem. Phys.*, 2010, **12**, 8016–8023.
5 A. Ishizaki, T. R. Calhoun, G. S. Schlau-Cohen and G. R. Fleming, *Phys. Chem. Chem. Phys.*, 2010, **12**, 7319–7337.
6 I. Azpiazu and N. Gautam, *J. Biol. Chem.*, 2004, **279**, 27709–27718.
7 A. Tigreros and J. Portilla, *RSC Adv.*, 2020, **10**, 19693–19712.
8 T. Zhang, I. E. Brumboiu, C. Grazioli, A. Guarnaccio, M. Coreno, M. de Simone, A. Santagata, H. Rensmo, B. Brena, V. Lanzilotto and C. Puglia, *J. Phys. Chem. C*, 2018, **122**, 17706–17717.
9 F. Monnier and M. Taillefer, *Angew. Chem., Int. Ed.*, 2009, **48**, 6954–6971.
10 T. Manifar and S. Rohani, *Can. J. Chem. Eng.*, 2004, **82**, 323–334.
11 X. Lian, Z. Zhao and D. Cheng, *Mol. Cryst. Liq. Cryst.*, 2017, **638**, 223–235.
12 O. Meth-Cohn and S. P. Stanforth, *Compr. Org. Synth.*, 1991, **2**, 777–794.
13 I. Reva, L. Lapinski, N. Chattopadhyay and R. Fausto, *Phys. Chem. Chem. Phys.*, 2003, **5**, 3844–3850.
14 P. Blanchard, C. Malacrida, C. Cabanetos, J. Roncali and S. Ludwigs, *Polym. Int.*, 2019, **68**, 589–606.
15 G. Meijer, G. Berden, W. L. Meerts, H. E. Hunziker, M. S. de Vries and H. R. Wendt, *Chem. Phys.*, 1992, **163**, 209–222.
16 P. Agarwala and D. Kabraa, *J. Mater. Chem. A*, 2017, **5**, 1348–1373.
17 A. Mahmood, *Sol. Energy*, 2016, **123**, 127–144.
18 E. Moulin, J. J. Armao IV and N. Giuseppone, *Acc. Chem. Res.*, 2019, **52**, 975–983.
19 E. Jaszczak, Ż. Polkowska, S. Narkowicz and J. Namieśnik, *Environ. Sci. Pollut. Res.*, 2017, **24**, 15929–15948.
20 D. Kanduti, P. Sterbenk and B. Artnik, *Mater Sociomed.*, 2016, **28**, 133–137.

Published on 14 February 2022. Downloaded by Bengal Engineering and Science University on 6/8/2022 1:03:11 PM.

21 P. Magee, *Side Eff. Drugs Annu.*, 2011, **33**, 479–490.
22 M. Luisa, G. Zamora and M. Manefield, *Rev. Environ. Sci. Biotechnol.*, 2010, **9**, 153–185.
23 M. Kumar and A. Puri, *Indian J. Occup. Environ. Med.*, 2012, **16**, 40–44.
24 S. K. Dey and C. Janiak, *RSC Adv.*, 2020, **10**, 14689–14693.
25 X. Zheng, W. Zhu, H. Ai, Y. Huang and Z. Lu, *Tetrahedron Lett.*, 2016, **57**, 5846–5849.
26 C. Chang, F. Wang, J. Qiang, Z. Zhang, Y. Chen, W. Zhang, Y. Wang and X. Chen, *Sens. Actuators, B*, 2017, **243**, 22–28.
27 B. Guo, H. Nie, W. Yang, Y. Tian, J. Jing and X. Zhang, *Sens. Actuators, B*, 2016, **236**, 459–465.
28 S. Wang, H. Xu, Q. Yang, Y. Song and Y. Li, *RSC Adv.*, 2015, **5**, 47990–47996.
29 F. Huo, J. Kang, C. Yin, J. Chao and Y. Zhang, *Sens. Actuators, B*, 2015, **21**, 593–598.
30 Y. Liu, D. Qiu, H. Pan, M. Li, H. Chen and H. Li, *J. Photochem. Photobiol., A*, 2018, **364**, 151–158.
31 Y. Zhao, L. Feng, X. Meng and J. Guan, *Dyes Pigm.*, 2020, **183**, 108713.
32 K. Deng, L. Wang, Q. Xia, R. Liu and J. Qu, *Sens. Actuators, B*, 2019, **296**, 126645.
33 E. Thanayupong, K. Suttisintong, M. Sukwattanasinitt and N. Niamnont, *New J. Chem.*, 2017, **41**, 4058–4064.
34 A. J. Benetoa and A. Siva, *Photochem. Photobiol. Sci.*, 2017, **16**, 255–261.
35 Q. Zhang, J. Zhang, H. Zuo, C. Wang and Y. Shen, *Tetrahedron*, 2016, **72**, 1244–1248.
36 S. Zhao, H. Liu, F. Wu and L. Zhu, *Chem. Lett.*, 2016, **45**, 570–572.
37 H. Wu, M. Chen, Q. Xu, Y. Zhang, P. Liu, W. Li and S. Fan, *Chem. Commun.*, 2019, **55**, 15137.
38 Q. Li, Z. Wang, W. Song, H. Ma, J. Dong, Y. Y. Quan, X. Ye and Z. S. Huang, *Dyes Pigm.*, 2019, **161**, 389–395.
39 A. Ozdemir and S. Erdemir, *J. Photochem. Photobiol., A*, 2020, **390**, 112328.
40 H. Muniyasamy, C. Chinnadurai, M. Nelson, A. M. Kubendra, K. Sukumaran, A. Balasubramaniem, M. Sepperumal, S. Ayyanar, M. Govindasamy, A. Ghfar and F. M. Alsubaie, *J. Mol. Liq.*, 2021, **334**, 116076.
41 B. Zuo, L. Liu, X. Feng, D. Li, W. Li, M. Huang and Q. Deng, *Dyes Pigm.*, 2021, **193**, 109534.
42 D. Tamilarasan, R. Suhasini, V. Thiagarajan and R. Balamurugan, *Eur. J. Org. Chem.*, 2020, **2020**, 993–1000.
43 K. Ghosh and I. Saha, *J. Inclusion Phenom. Macrocyclic Chem.*, 2011, **70**, 97–107.
44 Y. Qu, S. Qu, L. Yang, J. Hua and D. Qu, *Sens. Actuators, B*, 2012, **173**, 225–233.
45 K. Ponnuvel and V. Padmini, *J. Lumin.*, 2016, **169**, 289–294.
46 F. Wu, L. Wang, H. Tang and D. Cao, *Anal. Chem.*, 2019, **91**, 5261–5269.
47 C. H. Chen and M. Leung, *Tetrahedron*, 2011, **67**, 3924–3935.
48 S. Das, K. Aich, L. Patra, K. Ghoshal, S. Gharami, M. Bhattacharyya and T. K. Mondal, *Tetrahedron Lett.*, 2018, **59**, 1130–1135.
49 X. Chen, F. Wang, J. Y. Hyun, T. Wei, J. Qiang, X. Ren, I. Shin and J. Yoon, *Chem. Soc. Rev.*, 2016, **45**, 2976–3016.
50 S. Goswami, K. Aich, S. Das, B. Pakhira, K. Ghoshal, C. K. Quah, M. Bhattacharyya, H. K. Fun and S. Sarkar, *Chem.–Asian J.*, 2015, **10**, 694–700.
51 Y. Jiang, S. Zhang, B. Wang, T. Qian, C. Jin, S. Wu and J. Shen, *Tetrahedron*, 2018, **74**, 5733–5738.
52 X. Xu and Y. Qian, *Spectrochim. Acta, Part A*, 2017, **183**, 356–361.
53 Q. Zhang, P. Zhang, Y. Gong and C. Ding, *Sens. Actuators, B*, 2019, **278**, 73–81.
54 X. He, C. Xu, W. Xiong, Y. Qian, J. Fan, F. Ding, H. Deng, H. Chen and J. Shen, *Analyst*, 2020, **145**, 29–33.
55 W. Sun, Y. D. Shi, A. X. Ding, Z. L. Tan, R. Liu, R. Wang and Z. L. Lu, *Sens. Actuators, B*, 2018, **276**, 238–246.
56 X. Wang, W. Shi, L. Feng, J. Ma, Y. Li, X. Kong, Y. Chen, Y. Hui and Z. Xie, *Inorg. Chem. Commun.*, 2017, **79**, 50–54.
57 A. K. Mahapatra, G. Hazra, N. K. Das and S. Goswami, *Sens. Actuators, B*, 2011, **156**, 456–462.
58 H. Chen, P. Yang, Y. Li, L. Zhang, F. Ding, X. He and J. Shen, *Spectrochim. Acta, Part A*, 2020, **224**, 117384.
59 W. Li, Y. Zhang, X. Gan, M. Yang, B. Mie, M. Fang, Q. Zhang, J. Yu, J. Wu, Y. Tian and H. Zhou, *Sens. Actuators, B*, 2015, **206**, 640–646.
60 X. Gan, W. Li, C. Li, Z. Wu, D. Liu, B. Huang, H. Zhou and Y. Tian, *Sens. Actuators, B*, 2017, **239**, 642–651.
61 N. Lu, T. Jiang, H. Tan, Y. Hang, J. Yang, J. Wang, X. Qu and J. Hua, *Anal. Methods*, 2017, **9**, 2689–2695.
62 C. Pan, K. Wang, S. Ji, H. Wang, Z. Li, H. He and Y. Huo, *RSC Adv.*, 2017, **7**, 36007–36014.
63 L. Wang, X. Yang, X. Chen, Y. Zhou, X. Lu, C. Yan, Y. Xu, R. Liu and J. Qu, *Mater. Sci. Eng., C*, 2017, **72**, 551–557.
64 Y. Li, W. Shi, J. Ma, X. Wang, X. Kong, Y. Zhang, L. Feng, Y. Hui and Z. Xie, *J. Photochem. Photobiol., A*, 2017, **338**, 1–7.
65 Q. Zhang, J. Zhang, H. Zuo, C. Wang and Y. Shen, *Tetrahedron*, 2017, **73**, 2824–2830.
66 Q. Zhang, Y. Li, H. Zuo, C. Wang and Y. Shen, *J. Photochem. Photobiol., A*, 2017, **332**, 293–298.
67 F. Kolcu, D. Erdener and İ. Kaya, *Inorg. Chim. Acta*, 2020, **509**, 119676.
68 X. Wang, W. Shi, L. Feng, J. Ma, Y. Li, X. Kong, Y. Chen, Y. Hui and Z. Xie, *Inorg. Chem. Commun.*, 2017, **79**, 50–54.
69 A. K. Mahapatra, G. Hazra, N. K. Das and S. Goswami, *Sens. Actuators, B*, 2011, **156**, 456–462.
70 H. Chen, P. Yang, Y. Li, L. Zhang, F. Ding, X. He and J. Shen, *Spectrochim. Acta*, 2020, **224**, 117384.
71 W. Li, Y. Zhang, X. Gan, M. Yang, B. Mie, M. Fang, Q. Zhang, J. Yu, J. Wu, Y. Tian and H. Zhou, *Sens. Actuators, B*, 2015, **206**, 640–646.
72 S. Xie, S. Xia, Z. Xu, W. Li, E. Wang and S. Wang, *Synth. Met.*, 2021, **277**, 116784.
73 X. Gan, W. Li, C. Li, Z. Wu, D. Liu, B. Huang, H. Zhou and Y. Tian, *Sens. Actuators, B*, 2017, **239**, 642–651.
74 N. Lu, T. Jiang, H. Tan, Y. Hang, J. Yang, J. Wang, X. Qu and J. Hua, *Anal. Methods*, 2017, **9**, 2689–2695.
75 C. Pan, K. Wang, S. Ji, H. Wang, Z. Li, H. He and Y. Huo, *RSC Adv.*, 2017, **7**, 36007–36014.

 This journal is © The Royal Society of Chemistry 2022

Published on 14 February 2022. Downloaded by Bengal Engineering and Science University on 6/8/2022 1:03:11 PM.

76 L. Wang, X. Yang, X. Chen, Y. Zhou, X. Lu, C. Yan, Y. Xu, R. Liu and J. Qu, *Mater. Sci. Eng., C*, 2017, **72**, 551–557.
77 Y. P. Zhang, Q. Teng, Y. S. Yang, H. C. Guo and J. J. Xue, *Inorg. Chim. Acta*, 2021, **525**, 120469.
78 Y. Li, W. Shi, J. Ma, X. Wang, X. Kong, Y. Zhang, L. Feng, Y. Hui and Z. Xie, *J. Photochem. Photobiol., A*, 2017, **338**, 1–7.
79 Q. Zhang, J. Zhang, H. Zuo, C. Wang and Y. Shen, *Tetrahedron*, 2017, **73**, 2824–2830.
80 Q. Zhang, Y. Li, H. Zuo, C. Wang and Y. Shen, *J. Photochem. Photobiol., A*, 2017, **332**, 293–298.
81 L. Liu, J. Ma, J. Pan, D. Li, H. Wang and H. Yang, *New J. Chem.*, 2021, **45**, 5049–5059.
82 F. Kolcu, D. Erdener and İ. Kaya, *Inorg. Chim. Acta*, 2020, **509**, 119676.
83 F. Kolcu, D. Erdener and I. Kaya, *Synth. Met.*, 2021, **272**, 116668.
84 S. Erdemir and S. Malkondu, *Sens. Actuators, B*, 2013, **188**, 1225–1229.
85 P. S. Hariharan and S. P. Anthony, *Anal. Chim. Acta*, 2014, **848**, 74–79.
86 Y. Yang, B. Li, L. Zhang and Y. Guan, *J. Lumin.*, 2014, **145**, 895–898.
87 S. Malkondu and S. Erdemir, *Tetrahedron*, 2014, **70**, 5494–5498.
88 L. Wenfeng, M. Hengchang, L. con, M. Yuan, Q. Chunxuan, Z. Zhonwei, Y. Zengming, C. Haiying and L. Ziqiang, *RSC Adv.*, 2015, **5**, 6869.
89 A. Kundu and S. P. Anthony, *Spectrochim. Acta, Part A*, 2018, **189**, 342–348.
90 S. Sun, Q. Shu, P. Lin, Y. Li, S. Jina, X. Chen and D. Wang, *RSC Adv.*, 2016, **6**, 93826–93831.
91 S. Erdemir, *Sens. Actuators, B*, 2019, **290**, 558–564.
92 P. Thamaraiselvi, N. Duraipandy, M. Syamala Kiran and S. Easwaramoorthi, *ACS Sustainable Chem. Eng.*, 2019, **7**, 9865–9874.
93 J. Yao, Y. Fu, W. Xu, T. Fan, Y. Gao, Q. He, D. Zhu, H. Cao and J. Cheng, *Anal. Chem.*, 2016, **88**, 2497–2501.
94 K. Aich, S. Das, S. Gharami, L. Patra and T. K. Mondal, *New J. Chem.*, 2017, **41**, 12562–12568.
95 S. S. Ali, A. Gangopadhyay, A. K. Pramanik, U. N. Guria, S. K. Samanta and A. K. Mahapatra, *Dyes Pigm.*, 2019, **170**, 107585.
96 A. J. Beneto and A. Siva, *Sens. Actuators, B*, 2017, **242**, 535–544.
97 M. Hengchang, Z. Zhongwei, J. Yuanyuan, Z. Lajia, Q. Chunxuan, C. Haiying, Y. Zengming, Y. Zhiwang and Z. Lei, *RSC Adv.*, 2015, **5**, 87157–87167.
98 G. Sathiyan, B. Balasubramaniam, S. Ranjan, S. Chatterjee, P. Sen, A. Garg, R. K. Gupta and A. Singh, *Mater. Today Chem.*, 2019, **12**, 178–186.
99 L. Wenfeng, M. Hengchang and L. Ziqiang, *RSC Adv.*, 2014, **4**, 39351–39358.
100 S. Guo, J. Pan, J. Huang, L. Kong and J. Yang, *RSC Adv.*, 2019, **9**, 26043–26050.
101 Z. Luo, B. Liu, S. Si, Y. Lin, C. S. Luo, C. Pan, C. Zhao and L. Wang, *Dyes Pigm.*, 2017, **143**, 463–469.
102 K. Duraimurugan, R. Balasaravanan and A. Siva, *Sens. Actuators, B*, 2016, **231**, 302–312.
103 B. Zhao, B. Yang, X. Hu and B. Liu, *Spectrochim. Acta, Part A*, 2018, **199**, 117–122.
104 L. Xu, L. Ni, L. Sun, F. Zeng and S. Wu, *Analyst*, 2019, **144**, 6570–6577.
105 Q. Li, Z. Wang, M. Zhao, Y. Hong, Q. Jin, S. Yao, C. Zheng, Y. Y. Quan, X. Ye and Z. S. Huang, *Sens. Actuators, B*, 2019, **298**, 126898.
106 L. Wang, W. Yang, Y. Song and Y. Hu, *Spectrochim. Acta, Part A*, 2020, **243**, 118775.
107 X. Tang, W. Liu, J. Wu, W. Zhao, H. Zhang and P. Wang, *Tetrahedron Lett.*, 2011, **52**, 5136–5139.
108 Y. Duan, G. Ding, M. Yao, Q. Wang, H. Guo, X. Wang, Y. Zhang, J. Li, X. Li and X. Qin, *Spectrochim. Acta, Part A*, 2020, **236**, 118348.
109 Y. Xia, H. Zhang, X. Zhu, M. Fang, M. Yang, Q. Zhang, X. Li, H. Zhou, X. Yang and Y. Tian, *Dyes Pigm.*, 2019, **163**, 441–446.
110 Y. Chu, Z. Xie, Y. Yue, Y. Yue, X. Kong, W. Shi and S. Feng, *ACS Omega*, 2019, **4**, 5367–5373.
111 A. Karawek, P. Mayurachayakul, T. Santiwat, M. Sukwattanasinitt and N. Niamnont, *J. Photochem. Photobiol., A*, 2021, **404**, 112879.
112 S. K. Samanta, K. Maiti, S. S. Ali, U. N. Guria, A. Ghosh, P. Datta and A. K. Mahapatra, *Dyes Pigm.*, 2020, **173**, 107997.
113 X. Wang, G. Ding, Y. Duan, Y. Zhu, G. Zhu, M. Wang, X. Lia, Y. Zhang, X. Qin and C. H. Hungd, *Talanta*, 2020, **217**, 121029.
114 X. Wang, G. Ding, Y. Wang, S. Mao, K. Wang, Z. Ge, Y. Zhang, X. Li and C. H. Hung, *Tetrahedron*, 2020, **76**, 131726.